

Towards a Multimodal Charging Network: Joint Planning of Charging Stations and Battery Swapping Stations for Electrified Ride-Hailing Fleets

Zhijie Lai, Sen Li*

Department of Civil and Environmental Engineering, The Hong Kong University of Science and Technology, Clear Water Bay, Kowloon, Hong Kong

Abstract

This paper considers a multimodal charging network in which charging stations and battery swapping stations are jointly built to support an electric ride-hailing fleet synergistically. Our argument is based on the observation that charging an EV is a time-consuming burden, and battery swapping faces scaling issues due to its deployment costs. However, charging stations are cost-effective, making them ideal for scaling up EV fleets, while battery swapping stations offer quick turnaround and can be deployed in tandem with charging stations to improve fleet utilization and reduce operational costs. To fulfill this vision, we consider a ride-hailing platform that jointly builds charging and battery swapping stations to support an EV fleet. An optimization model is proposed to capture the platform's planning and operational decisions. In particular, the model incorporates essential components such as elastic passenger demand, spatial charging equilibrium, charging and swapping congestion, etc. The overall problem is formulated as a nonconcave program. Instead of pursuing the globally optimal solution, we establish a tight upper bound through relaxation and decomposition, allowing us to evaluate the solution optimality even in the absence of concavity. Through case studies for Manhattan, New York City, we find that joint planning of charging and battery swapping stations outperforms deploying only one of them, yielding a total profit that is 11.7% higher than swapping-only deployment under a limited budget, and 17.5% higher than charging-only deployment under a sufficient budget. These results underscore the complementary benefit between charging and battery swapping facilities.

Keywords: infrastructure planning, plug-in charging, battery swapping, electric vehicle, ride-hailing

1. Introduction

The electrification of transportation is essential for establishing a green and sustainable mobility future. In recent years, governments worldwide have committed to supporting the adoption of electric vehicles (EVs) through a suite of regulations and subsidies. Among all types of vehicles, commercial fleets (e.g., ride-hailing cars) are viewed as a promising sector for transport electrification due to their higher annual mileage. Companies like Uber and Didi, with their extensive global operations, have the potential to drive significant progress in pollution reduction. Uber alone provides approximately 21 million rides per day across over 10,000 cities [1], while Didi's global daily trips can even exceed 50 million [2]. However, the vast majority of these rides are delivered by fossil fuel vehicles, with EVs accounting for less than 5% of Uber drivers' miles driven in Europe [3], and less than 0.5% in the US [4]. In fact, the environmental benefits of electrifying ride-hailing fleets are estimated to be three times higher than those of electrifying private cars [5]. To

*Corresponding author

Email addresses: zlaiaa@connect.ust.hk (Zhijie Lai), cesli@ust.hk (Sen Li)

unlock this enormous potential, California regulators have passed a legislation requiring transportation network companies to transition from petroleum to electric vehicles by 2030 [6]. In response, both Uber and Lyft have pledged to offer zero-emission mobility-on-demand services by the end of the decade [7][8].

However, charging infrastructure remains a persistent barrier that hinders the electrification of ride-hailing fleets in the long term. Unlike private cars, commercial fleets need to run on the road as long as possible to accrue profits, while most ride-hailing EV drivers need to top up the batteries once or twice every day due to the limited battery range [9]. The frequent need for charging, coupled with the longer charging time compared to refueling a gas-powered vehicle, results in significant downtime, incurring a substantial opportunity cost for the drivers [10]. This makes EVs less appealing for ride-hailing use. As per [11], charging time comprises 72-75% of the total downtime spent on charging trips. This indicates that charging time, rather than travel time or waiting time, is the dominant bottleneck for EV charging, even with a dense charging station network. While fast charging can alleviate this issue, it typically relies on high voltage and draws substantial power from the grid. Massively deploying fast chargers in densely populated urban areas is impractical due to the potential voltage drop and instability it can cause in the already strained power distribution network. Additionally, upgrading the power distribution infrastructure to support such high-power charging can be prohibitively expensive. As a result, plug-in charging stations presents an inherent bottleneck for the ride-hailing industry: regardless of the density of the charging network, there is always a significant downtime for the commercial fleet due to the limited charging speed that can be maximally supported by the capacity of existing power distribution networks in large metropolitan areas. This leads to low fleet utilization and high operational costs for the ride-hailing platform, thereby limiting the economic viability of electrifying ride-hailing fleets.

Battery swapping is an alternative method for recharging depleted EVs, where an empty battery is replaced with a fully charged one in a few minutes. There was a heated debate over plug-in charging and battery swapping, after which many western countries predominantly invested in charging stations instead of battery swapping stations. One primary reason for this preference is the lack of standardized batteries among EV manufacturers. In contrast, China has taken a more impartial stance, encouraging both plug-in charging and battery swapping technologies. This policy is based on the belief that, standardizing batteries is more feasible for commercial vehicles than for privately-owned EVs. In recent years, governments are pushing electrification among taxi fleets, which naturally come with a unified battery model (see Shenzhen [12] for an example). In the private sector, ride-hailing platforms have actively collaborated with automobile manufacturers to produce affordable EVs tailored for ride-hailing services. Notable examples include the battery-swappable Cao Cao 60 [13], a joint effort between Caocao Mobility and Geely, and the D1 [14], co-developed by Didi and BYD. Uber is also working with automakers to develop custom-made EVs for ride-hailing and delivery applications [15]. Large-scale deployment of these customized EVs can naturally address the compatibility issue, making battery swapping a viable solution. Furthermore, future mobility-on-demand systems are envisioned to be driven by electric and autonomous vehicles that operate under the centralized control of the platform. In fact, both Uber and Didi have announced their plans to offer services using robotaxis [16][17]. This important trend further justifies a unified battery standard and the feasibility of battery swapping. The advantages of battery swapping can be tremendous for electric ride-hailing fleets. It enables faster recharge compared to even the fastest chargers, which can substantially reduce charging downtime, improve fleet utilization, and thereby enhance business sustainability. In this regard, battery swapping is a competitive solution for large commercial fleets and is attracting increasing attention from the industry recently. For instance, BP has partnered with Chinese battery swapping specialist Aulton to offer services for taxis, ride-hailing vehicles, and other passenger cars [18]. San Francisco-based startup Ample provides battery swapping services for Uber and other commercial EVs using modular power packs. They estimate that a ride-hailing driver only needs to spend 3.6 hours per week charging their EV using battery swapping, which is 86% less time than using fast charging [19]. Nevertheless, we must recognize that scaling a battery swapping network requires a longer timeline due to the higher deployment costs.

To capitalize on the advantages of plug-in charging and battery swapping, we propose a *multimodal charging network* in which charging stations and battery swapping stations are jointly built to support a ride-hailing EV fleet. Our central thesis is predicated on the observation that charging stations are cost-effective, making them ideally suitable for scaling up EV adoption in the beginning, while battery swapping stations offer quicker turnaround and can be deployed in tandem with charging stations to improve fleet utilization and reduce operational costs. To realize this vision, we consider a multi-stage infrastructure planning problem in which a profit-maximizing platform jointly deploys charging and battery swapping stations with a limited budget and simultaneously provides ride-hailing services over a transportation network. An optimization model is proposed to decide when and where to deploy each type of charging facilities, along with the ride-hailing operational decisions such as pricing strategies. The key contributions of this paper are summarized as follows:

1. This paper examines the benefits of a multimodal charging network consisting of both charging stations and battery swapping stations, with an emphasis on exploring their synergistic benefits. Despite extensive research on charging infrastructure planning, the complementary effects between these two facilities have been overlooked in the existing literature. To the best of our knowledge, this paper makes the first attempt to investigate the multimodal charging network for ride-hailing EV fleets by considering the joint deployment of charging stations and battery swapping stations.
2. We propose a multi-stage charging network expansion model to capture the coupled infrastructure planning and operational decisions in a ride-hailing network. This model integrates fundamental elements, including demand elasticity, drivers' charging behavior, charging and swapping waiting times, and their dependence on fleet status and charging infrastructure. Specifically, the stationary charging demand is analytically derived given passenger demand patterns and vehicle flows. The congestion at different facilities is captured by queuing-theoretic models, and drivers' decisions on charging location and mode are characterized by a spatial charging equilibrium model.
3. We establish a tight upper bound for the joint deployment problem despite its nonconcavity. A decomposable problem is developed through proper model relaxations. By leveraging the favorable structures of the relaxed problem, we are able to obtain an accurate estimation of the globally optimal solution to the original problem, enabling us to verify the optimality of the solution obtained. We show that our approach provides a high-quality upper bound with an optimality gap of around 3%.
4. Through extensive numerical studies, we evaluate the effectiveness of joint deployment and gain valuable insights into infrastructure planning. We find that joint planning of charging and battery swapping stations can harness the complementary benefits of the two facilities, leading to improved profit and reduced charging costs. In particular, based on a case study for Manhattan, New York City, the total profit of joint planning is 11.7% higher than swapping-only deployment under a tight budget, and 17.5% higher than charging-only deployment under a generous budget. Furthermore, compared to charging-only deployment, joint planning yields a charging cost reduction of 18.8% under a limited budget and 44.4% under a sufficient budget. However, a multimodal charging network may result in a higher volume of cross-zone traffic than a unimodal charging network due to driver's charging behaviors, which reveals the potential impacts of infrastructure planning on urban traffic congestion and management.

2. Literature Review

2.1. Modeling Electric Ride-Hailing Markets

In ride-hailing markets, EV fleets differ from the gasoline-powered one in that EV charging would intermittently interrupt services and result in lengthy downtime, which impacts the platform's operation and necessitates special consideration in the formulation of mathematical models, the design of operational strategies, as well as the formation of regulatory policies.

One of the key topics for electric ride-hailing markets is the charging and operational strategies for EVs. Many studies focus on capturing the distinct driving patterns of ride-hailing EV drivers. For instance, Ke et al. [20] modeled drivers' behavior in a ride-sourcing market with EVs and gasoline vehicles, developed a time-expanded network to sketch out drivers' working and recharging schedules, and found that passengers, drivers, and the platform are all worse off when the charging price increases. Qin et al. [21] used a multi-state model to identify two distinct driving patterns for ride-hailing EVs, which outline when, for how long, and under what state of charge a driver will decide to recharge an EV. Alam [22] emulated the daily trip patterns of ride-sourcing EVs using an optimization-based method and investigated the induced charging demand using agent-based simulation. Besides, a growing body of literature highlights the operations of electric ride-hailing markets. Shi et al. [23] formulated a dynamic vehicle routing problem (VRP) to capture the operations of a ride-hailing EV fleet and solved the problem using reinforcement learning. Kullman et al. [24] also employed deep reinforcement learning to develop operational policies for ride-hailing EVs, including vehicle assignment, charging, and repositioning decisions. Pricing strategies are considered in [25], where Hong and Liu examined the optimal price and wage of green ride services while taking into account the opportunity cost of EV drivers as well as passengers' willingness to pay for eco-friendly trips. Ding et al. [26] considered the integration of ride-hailing and vehicle-to-grid (V2G) services and developed a game-theoretic framework to characterize the market equilibrium. Cai et al. [27] investigated the operations of integrated ride-sourcing and EV charging services in a nested two-sided market framework. Furthermore, related research is expanded into shared autonomous electric vehicles (SAEVs) [28][29][30][31]. Among others, Turan et al. [29] considered pricing, routing, and charging strategies. Yi and Smart [30] focused on joint dispatching and charging management. Al-Kanj et al. [31] used approximate dynamic programming to develop high-quality pricing, dispatching, repositioning, charging, and fleet sizing strategies for the operations of an SAEV fleet.

Another important topic is on policies aimed at promoting the electrification of the ride-hailing industry. Different policy options have been explored in the literature, with a primary focus on pricing incentives that includes subsidy for EV purchases, incentive schemes for EV rental, and financial support to infrastructure supply [4][10][32][33][34][35]. Particularly, Liu et al. [10] examined the market response and electrification levels under three different regulatory policies, including annual permit fees, differential trip-based fees, and differential commission caps. They indicated that the last policy is the most cost-efficient and can simultaneously benefit drivers and passengers. Slowik et al. [32] also found that well-designed taxes and fee structures can make EVs the most economically attractive technology for ride-hailing fleets. As per [35], governments should shift the target of current subsidies to the most intensively-used vehicles and the people most in need of financial support, for instance, ride-hailing drivers. And ensuring access to overnight charging is another crucial step to dismantling barriers to vehicle electrification. However, Mo et al. [33] showed that given a limited budget, governments should subsidize charging infrastructure before supporting EV purchase. In summary, all aforementioned works focus on the operational strategies and/or public policies for electric ride-hailing fleets, while the planning of charging infrastructure for the ride-hailing network is not explicitly considered.

2.2. Infrastructure Planning for EV fleets

Charging infrastructure is a crucial component in a green and sustainable mobility ecosystem. In the existing literature, the planning strategies of EV infrastructure, including both charging stations and battery swapping stations, have been extensively examined (see [36] for a comprehensive summary). Unlike private EVs that typically charge at home, commercial EV fleets have significantly higher mileage and rely heavily on public charging stations, requiring extra infrastructure planning considerations. In light of this, we review relevant studies that focus on infrastructure planning for commercial EV fleets, such as those in electric ride-hailing markets.

A recurrent topic in the literature is planning charging stations for EV fleets that offer mobility-on-demand

services over the transportation network. Brandstätter et al. [37] studied optimal locations of charging stations for a car-sharing EV fleet considering demand stochasticity. Roni et al. [11] tackled charging station allocation and car-sharing EV assignment in a joint optimization framework and confirmed that charging time is a dominant component of the total fleet downtime. Ma and Xie [38] also jointly considered infrastructure planning and vehicle assignment problem for ride-hailing EVs and formulated a bi-level problem to minimize the charging operation time. Alam and Guo [39] took drivers’ value of time into account in planning charging stations for ride-hailing EVs. Bauer et al. [40] adopted agent-based simulation to analyze charging infrastructure for electrified ride-hailing fleets and suggested that the cost of charging infrastructure accounts for a small fraction of the total cost of an electric ride-hailing trip. Following Lyft’s announcement to reach 100% EVs, Jenn [41] examined the infrastructure deployment necessary to meet charging demand from fully-electrified fleets in California and found that a shift from daytime charging to overnight charging can significantly reduce costs.

The planning of battery swapping stations also attracts a lot of research focus. Mak et al. [42] developed a robust optimization framework to deploy battery swapping facilities and investigated how battery standardization and technology advancements will impact the optimal deployment strategy. Targeted at refueling electric taxicabs, Wang et al. [43] jointly tackled the deployment of battery swapping stations and charging scheduling of EV fleets and designed a planning scheme to decrease in-station queuing time and improve quality of service of the taxicab fleet. Infante et al. [44] considered stochastic charging demand and formulated a two-stage optimization with recourse, where battery swapping stations are deployed in the planning stage and the infrastructure network is coordinated in the operation stage. Further, Yang et al. [45] proposed a data-driven approach to deploying and operating battery swapping stations with centralized management. Moon et al. [46] examined the locating problem of battery swapping stations in a passenger traffic network to achieve the seamless operation of electric buses.

Despite a large volume of literature on charging infrastructure planning for electric ride-hailing fleets, most existing works focus on either charging or battery swapping stations, without considering their complementary effects. Among the few early attempts, Zhang et al. [47] studied the joint planning of swapping and charging stations for private EVs, and Zhang et al. [48] explored the charging demand management for electric taxis in the presence of a hybrid infrastructure network. In contrast, this paper distinguishes itself from all previous studies in two key aspects. Firstly, we consider a multimodal charging network where charging stations and battery swapping stations are jointly deployed to overcome their respective limitations and elicit the synergy value. Secondly, we integrate infrastructure planning decisions and operational decisions of the ride-hailing platform within a unified framework to account for their interdependence. To the best of our knowledge, these considerations have not been studied in the literature.

3. Mathematical Formulation

We consider a platform that offers on-demand ride-hailing services using an EV fleet over a transportation network. To facilitate EV charging, the platform collaborates with charging infrastructure providers to devise a long-term infrastructure deployment strategy spanning T stages,¹ each corresponding to a duration of 1-2 year, while subject to a limited budget.² At each stage, the platform determines how many charging stations and/or battery swapping stations to build, where to deploy charging infrastructure, and how

¹This is to emulate a coalition of ride-hailing platforms and infrastructure providers, which follows the industry practice. For example, Didi and BP also join forces to build an EV charging network in China [49]. Charging network provider Wallbox partners with Uber to install charging stations for Uber drivers [50]. Ample teams up with Sally, an EV fleet operator, to deploy swapping stations for ride-hailing and other service vehicles in metropolitan cities in the US [51].

²The budget may come from government financial subsidies aimed at promoting charging infrastructure development, which is common in various jurisdictions [52][53].

to price ride-hailing services under the existing infrastructure network, etc. Note that infrastructure planning decisions are typically made on a timescale of years, whereas operational decisions, influenced by time-varying travel demand, impact market outcomes on a much shorter timescale, ranging from minutes to hours. In this light, the steady-state equilibrium at each stage is assumed to inform infrastructure planning. This assumption is commonly made in many existing works on ride-hailing markets [10][54][38]. The remainder of this section details a mathematical model for the optimal deployment of a multimodal charging network.

3.1. Charging Network Expansion

The platform deploys a multimodal charging network in a city consisting of multiple zones. Let $x_{i,t}^k$ denote the number of charging/swapping stations built in zone i up to stage t , where $k \in \mathcal{K} = \{c, s\}$ is the index of facility mode, with c and s representing charging and swapping stations, respectively. Note that the planning decisions $x_{i,t}^k$ are considered continuous in this study, which suffices to evaluate the effectiveness of joint planning while also simplifying the solution process. Infrastructure deployment is subject to the budgetary constraint:

$$\sum_{i \in \mathcal{I}} \sum_{k \in \mathcal{K}} \gamma_k x_{i,t}^k \leq b_t, \quad (1)$$

where γ_k is the unit deployment costs for different facilities, b_t is the cumulative budget as of stage t , \mathcal{I} is the set of zones, and $\mathcal{T} = \{1, \dots, T\}$ is the set of stages within the planning horizon. This constraint implies that any unused budget during stage t can be allocated to future stages. Define $x_{i,0}^k$ as the initial number of facilities. The expansion of charging network complies the following relation:

$$x_{i,t}^k - x_{i,t-1}^k \geq 0, \quad (2)$$

indicating that the charging infrastructure built at each stage will be available for future use.

Given the infrastructure network at each stage t , the platform determines its operational strategies for profit maximization. These decisions involve both the supply and demand sides of ride-hailing markets, which are intimately coupled with infrastructure planning. To characterize this intrinsic correlation, we observe that the impacts of ride-hailing operations can be analyzed in the following sequence: (a) the platform set service prices over the transportation network to steer passenger demand; (b) passenger demand induces a flow pattern of EVs and generates a spatial distribution of charging demand; (c) drivers strategically decide charging locations and modes to minimize their individual charging downtime, leading to an equilibrium stage; (d) drivers' charging behavior, in turn, affects the total downtime of the entire fleet, thereby influencing infrastructure planning decisions. In subsequent subsections, we will present the platform's operational decisions following the aforementioned sequence.

3.2. Passenger Demand Management

Ride-hailing passengers are sensitive to price and waiting time. We denote the ride fare for a trip from zone i to j at stage t as $p_{ij,t}$, and the average waiting time before each passenger is picked up as $w_{i,t}^p$. The arrival rate of passengers can be represented as:

$$q_{ij,t} = \bar{q}_{ij} F_p \left(p_{ij,t} + \beta w_{i,t}^p \right), \quad (3)$$

where \bar{q}_{ij} is the total travel demand from zone i to j , including all passengers regardless of travel modes; β is passengers' value of time; and $F_p(\cdot)$ is a strictly decreasing function representing the proportion of travelers using ride-hailing services. Since $F_p(\cdot)$ is strictly decreasing, it is invertible and the price $p_{ij,t}$ can be expressed as a function of $q_{ij,t}$ and $w_{i,t}^p$. Note that for a given $w_{i,t}^p$, the revenue, $p_{ij,t} q_{ij,t}$, is known to be

concave in the demand rate $q_{ij,t}/\bar{q}_{ij}$ for various demand functions, such as linear, exponential, logit, and others [55]. This property will be leveraged to facilitate the derivation of our proposed upper bounds. We therefore use the demand for each OD pair $q_{ij,t}$ as a decision variable in place of the price $p_{ij,t}$ hereinafter.

Assuming a first-come-first-serve matching principle, where the platform promptly assigns each rider to the nearest available vehicle, Passengers' waiting time only depends on the number of idle vehicles, denoted as $N_{i,t}^v$. This waiting time $w_{i,t}^p$ can be captured by the well-established square root law [56][57]:

$$w_{i,t}^p = \frac{\phi}{\sqrt{N_{i,t}^v}}, \quad (4)$$

where ϕ is a model parameter depending on the geometry of the city. This functional form is intuitive. As the number of idle vehicles increases subject to a fixed spatial distribution, the distance between a passenger and each of the vehicles will decrease in proportion to the square root of the number of idle vehicles. A rigorous proof for the case of uniform distribution can be found in [57]. Note that the first-come-first-serve matching mechanism is a common assumption in the existing literature on ride-hailing markets [58][59][33][54]. We believe that it does not limit the model's generality since as the proposed methodology in this paper does not hinge on the square root structure of (4).

Due to the asymmetric passenger demand, the platform further dispatches vehicles from one zone to another to relocate the fleet. Let $r_{ij,t}$ denote the rebalancing flow from zone i to j . In the long run, the vehicle inflow and outflow in each zone should be equal, leading to the following flow balance constraint:

$$\sum_{j \in \mathcal{I}} (q_{ij,t} + r_{ij,t}) = \sum_{j \in \mathcal{I}} (q_{ji,t} + r_{ji,t}), \quad (5)$$

where the left-hand side represents the total flow leaving zone i , and the right-hand side denotes the total flow entering zone i .

3.3. Potential Charging Demand

The stationary distribution of charging demand refers to the long-run probability of an EV requiring recharging in each zone. In this study, we assume that each driver will recharge the EV when its state of charge falls below a random threshold, with a mean value ε . As a result, a certain proportion of EVs will run out of power in each zone in the long run. Note that different EV drivers may adopt different charging schedules, characterized by distinct threshold values. However, when examining the stationary charging demand, we only need to focus on the average value of this threshold. We further assume that prior to reaching the threshold, the movement of an EV across the transportation network is completely governed by random passenger demand and is not affected by the specific threshold value. Consequently, the spatial distribution of charging demand aligns with the equilibrium fleet distribution, which, in turn, depends on the movement of the EV fleet and is inherently influenced by the platform's operational decisions.

Following the idea in [60], we consider the EV fleet movement as a random walk with a certain transition matrix P . To derive the transition matrix, we first note that the operating hours of EVs consist of idle trips (waiting for the next passenger), pickup trips (heading to pick up an assigned passenger), delivery trips (transporting passengers to destinations), and rebalancing trips (relocating from one zone to another with empty seats). The first two categories are regarded as intra-zone trips, while the last two types can be either inter-zone or intra-zone trips depending on destinations. In this light, we define $D_{ij,t}$ to capture the average number of EVs that travel from zone i to zone j (either with or without a passenger):

$$D_{ij,t} = \begin{cases} N_{i,t}^v + \sum_{j' \in \mathcal{I}} q_{ij',t} w_{i,t}^p + q_{ij,t} t_{ij} + r_{ij,t} t_{ij}, & i = j, \\ q_{ij,t} t_{ij} + r_{ij,t} t_{ij}, & i \neq j. \end{cases} \quad (6a)$$

$$(6b)$$

The last three terms in (6a) follow the Little's law and respectively represent the number of EVs undergoing pickup, delivery, and rebalancing trips. With this information, we can compute the transition matrix P_t :

$$P_{ij,t} = \frac{D_{ij,t}}{\sum_{j \in \mathcal{I}} D_{ij,t}}, \quad (7)$$

which captures the probability of an EV departing for zone j given that it is currently in zone i . Let $n_{i,t} > 0$ denote the probability of an EV staying in each zone at equilibrium. Based on the above analysis, the row vector $n_t = [n_{i,t}]_{i \in \mathcal{I}}$ further represents the stationary charging demand distribution and thus satisfies $\sum_{i \in \mathcal{I}} n_{i,t} = 1$. The derivation of this distribution follows the proposition below:

Proposition 1. *For any $q_{ij,t} > 0, \forall i, j \in \mathcal{I}$ and the corresponding transition matrix $P_t = [P_{ij,t}]_{i,j \in \mathcal{I}}$, the stationary charging demand distribution n_t exists and is uniquely given by*

$$n_t P_t = n_t. \quad (8)$$

Proof. Since $q_{ij,t} > 0$, we know that P_t is element-wise strictly positive. Additionally, every row of P_t adds to 1, so it is a row stochastic matrix. According to the Perron–Frobenius theorem [61], P_t has an eigenvalue 1 and the corresponding left eigenvector is unique and has all-positive entries. As a result, solving (8) yields a unique stationary charging demand distribution n_t . \square

The assumption of strict positivity for $q_{ij,t}$ is a mild one as it only requires the platform to provide services for each OD pair. Given n_t , we further define $\Lambda_{i,t}$ as the potential charging demand in each zone induced by EV movement, which clearly satisfies:

$$\Lambda_{i,t} = n_{i,t} \sum_{j \in \mathcal{I}} \Lambda_{j,t}. \quad (9)$$

This potential charging demand $\Lambda_{i,t}$ can be accommodated by charging or battery swapping stations located in different zones. When an EV needs to recharge, the driver decides the charging location and mode. Let $f_{ij,t}^k$ denote the EV flow traveling from zone i to j to recharge using mode k at stage t . Consequently, the potential charging demand $\Lambda_{i,t}$ can be expressed as the sum of these flows:

$$\Lambda_{i,t} = \sum_{j \in \mathcal{I}} \sum_{k \in \mathcal{K}} f_{ij,t}^k. \quad (10)$$

Let ω denote the average rate of electricity consumption, and let Ω denote the average battery capacity. At equilibrium, the electricity consumed by the entire EV fleet should match the total energy replenished through plug-in charging and battery swapping. This leads to the following energy balance condition:

$$\omega \left[\sum_{i \in \mathcal{I}} N_{i,t}^v + \sum_{i \in \mathcal{I}} \sum_{j \in \mathcal{I}} q_{ij,t} w_{i,t}^p + \sum_{i \in \mathcal{I}} \sum_{j \in \mathcal{I}} q_{ij,t} t_{ij} + \sum_{i \in \mathcal{I}} \sum_{j \in \mathcal{I}} r_{ij,t} t_{ij} + \sum_{i \in \mathcal{I}} \sum_{j \in \mathcal{I}} \sum_{k \in \mathcal{K}} f_{ij,t}^k t_{ij} \right] = (1 - \varepsilon) \Omega \sum_{i \in \mathcal{I}} \Lambda_{i,t} \quad (11)$$

where t_{ij} is the travel time from zone i to j and ε is the average energy threshold below which an EV will top up the battery. In (11), the left-hand side is derived from Little's law and represents the total energy consumption, while the right-hand side represents the power input to the entire fleet. The terms on the left-hand side account for the energy consumed by EVs that are idling, picking up passengers, delivering passengers, relocating, and en-route to recharge, respectively.

So far, we have characterized how the platform's operational decisions affect the potential charging demand. Specifically, (8) reveals the equilibrium spatial distribution of charging demand, while (11) provides a scaling factor for (8) to ensure a balanced energy input and output. It is important to note that the potential charging demand is endogenous in the sense that it depends on the transition matrix P_t , which further depends on the platform's operational decisions.

Remark 1. Ideally, charging flows $f_{ij,t}^k$ are part of the vehicle movement and can impact the equilibrium fleet distribution. Therefore, they should be included in (6) when deriving the transition matrix P_t . However, incorporating charging flows in this way would result in a more complex model with compromised tractability. As a result, we have decided to simplify the model by assuming that the transition matrix is independent of charging flows. We acknowledge that this simplification is a limitation of our proposed model and recognize the potential for some deviation in the results. However, we argue that this deviation turns out to be insignificant since charging flows typically represent a small fraction of the total EV movement. In a realistic simulation study, we find that the deviation of charging demand distributions due to the neglect of charging flows $f_{ij,t}^k$ in (6) is less than 0.1% (measured by L2 distance). Hence, we leave the development of a more comprehensive model that incorporates charging flows in the transition matrix as an avenue for future research.

3.4. Spatial Charging Equilibrium

Given the potential charging demand, drivers make strategic decisions regarding where to recharge and which charging mode to use so as to minimize their charging costs. The aggregate choices of drivers, characterized by the charging flow $f_{ij,t}^k$, collectively establish a spatial charging equilibrium across different zones. To formally capture this equilibrium, we first introduce the notion of actual charging demand:

$$\lambda_{i,t}^k = \sum_{j \in \mathcal{I}} f_{j,i,t}^k, \quad (12)$$

which defines the total demand for charging facilities of mode k in zone i at stage t . In addition, the charging cost of each EV driver consists of the travel time to the selected zone, the waiting time at the visited facility, and the service time of the chosen charging mode:

$$c_{ij,t}^k = t_{ij} + t_k + w_{j,t}^k(x_{j,t}, \lambda_{j,t}^k). \quad (13)$$

Here, t_k corresponds to the service time associated with mode k , and $w_{j,t}^k$ denotes the queueing time, which is a function of facility supply $x_{j,t}$ and charging demand $\lambda_{j,t}^k$. The precise relationship between $w_{j,t}^k$ and $x_{j,t}$, as well as $\lambda_{j,t}^k$, will be elaborated upon in the subsequent subsection. We then introduce the definition of spatial charging equilibrium:

Definition 3.1 (Spatial Charging Equilibrium). The system is said to reach spatial charging equilibrium when no EV driver from the same zone can reduce her charging cost by unilaterally deviating from the selected charging location or mode.

Based on this definition, the equilibrium conditions can be equivalently expressed as

$$\begin{cases} f_{ij,t}^k \geq 0, & (14a) \\ c_{ij,t}^k - u_{i,t} \geq 0, & (14b) \\ f_{ij,t}^k (c_{ij,t}^k - u_{i,t}) = 0, & (14c) \end{cases}$$

together with the flow conservation constraint (10), where $u_{i,t}$ denotes the equilibrium charging cost for each EV from zone i at stage t . These conditions state that if an EV travels from zone i to j to recharge using mode k , the associated charging cost is equal to the equilibrium cost for zone i , while those not selected location and mode will incur a charging cost greater than or at least equal to the equilibrium cost $u_{i,t}$. Thereby, if the flow pattern $f_{ij,t}^k$ satisfies these conditions, no drivers can be better off by unilaterally changing their decisions.

3.5. Queueing Time at Stations

This subsection will detail the waiting times at charging and battery swapping stations. We proceed by first assuming that different facilities are uniformly distributed within each zone, and that EV drivers only strategically determine the zone and mode for recharging, but will always visit the closest facility of the selected mode. Therefore, the average arrival rate of EVs for each facility of mode k is $\bar{\lambda}_{i,t}^k = \lambda_{i,t}^k/x_{i,t}^k$.

Queueing time at charging stations: Assuming the arrival of EVs follows a Poisson distribution with rate $\bar{\lambda}_{i,t}^c$ and the charging time follows an exponential distribution with an average value of t_c , we can model the charging process as an $M/M/C/K$ queue. Here, C represents the capacity of each charging station (i.e., the number of chargers), and K represents the queue capacity (i.e., only a maximum of K customers are allowed to stay in the queue). The mean queue length for this queueing system is well-established [62] and can be expressed as:

$$L_c = \frac{\rho P_0 (\bar{\lambda}_{i,t}^c t_c)^C}{C!(1-\rho)^2} [1 - \rho^{K-C+1} - (1-\rho)(K-C+1)\rho^{K-C}], \quad (15)$$

where $\rho = \bar{\lambda}_{i,t}^c t_c / C$, and

$$P_0 = \begin{cases} \left[\frac{(\bar{\lambda}_{i,t}^c t_c)^C}{C!} \frac{1 - \rho^{K-C+1}}{1 - \rho} + \sum_{a=0}^{C-1} \frac{(\bar{\lambda}_{i,t}^c t_c)^a}{a!} \right]^{-1}, & \text{if } \rho \neq 1, \\ \left[\frac{(\bar{\lambda}_{i,t}^c t_c)^C}{C!} (K - C + 1) + \sum_{a=0}^{C-1} \frac{(\bar{\lambda}_{i,t}^c t_c)^a}{a!} \right]^{-1}, & \text{if } \rho = 1. \end{cases} \quad (16a)$$

Note that if $\rho = 1$, L'Hôpital's rule should be applied twice to the expression of L_c . Due to the limited queue capacity, new arrivals will be blocked if the queue is full. The blocking rate is given by

$$P_K = \frac{(\bar{\lambda}_{i,t}^c t_c)^K}{C! C^{K-C}} P_0. \quad (17)$$

The average waiting time at each charging station can thus be obtained by applying Little's law:

$$w_{i,t}^c = \frac{L_c}{\bar{\lambda}_{i,t}^c (1 - P_K)}. \quad (18)$$

Queueing time at swapping stations: Compared to charging stations, battery swapping stations have much more complex dynamics. If fully-charged batteries are available when an EV arrives, it will be immediately maneuvered into a changeover bay for battery replacement. Otherwise, EVs will queue up for the next fully-charged power pack as long as the queue is not full upon arrival. The depleted batteries will be plugged in right after being removed from EVs. To model these dynamics, we adopt the framework in [63] and formulate the system as a mixed queueing network. As illustrated in Figure 1, the queueing network includes an open queue for EVs and a closed queue for batteries. The former captures the arrival and departure of EVs, while the latter models the circulation of batteries. The battery queue is considered closed because the arrival of depleted batteries and the departure of fully-charged batteries are in one-to-one correspondence. Consequently, each station maintains a fixed number of batteries in circulation.

To ensure consistency and fair comparison between the two facilities, we consider each swapping station is equipped with C chargers for recharging depleted batteries and has a queue capacity of K . Additionally, we denote S as the number of automated swapping slots, B as the number of batteries in circulation, and t_s as the constant service time for each swap. The arrival of EVs at each swapping station is also assumed

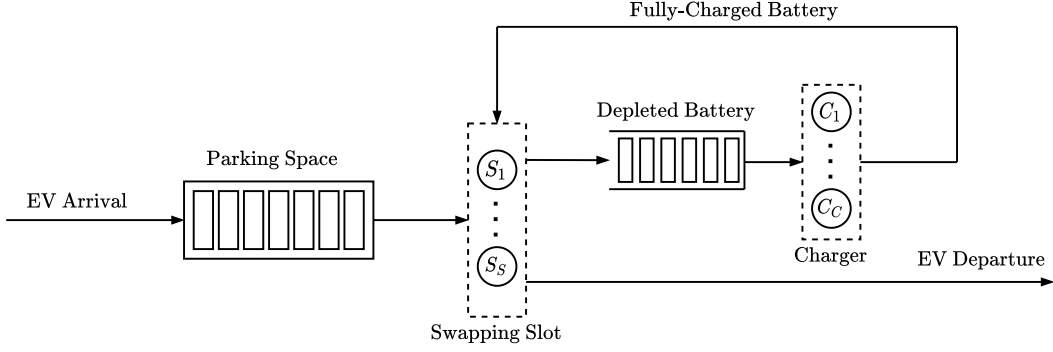


Figure 1: The mixed queueing network for a battery swapping station.

to be Poisson with rate $\bar{\lambda}_{i,t}^s$. Define $g(u)$ as the probability of having u new-coming EVs during any time interval $(t, t + t_s]$. Based on the probability mass function of Poisson distribution, we derive $g(u)$ as follows:

$$g(u) = \frac{(\bar{\lambda}_{i,t}^s t_s)^u \exp(-\bar{\lambda}_{i,t}^s t_s)}{u!}, \quad u \geq 0. \quad (19)$$

Further let $f(u, v)$ represent the probability of having v batteries complete charging during $(t, t + t_s]$ provided that there are u batteries being charged at time t . Clearly, $f(u, v)$ is supported on $u \in [0, C]$ and $v \in [0, u]$. As aforementioned in the charging queue, suppose the battery charging time follows an independent and identical exponential distribution with mean t_c . Then $f(u, v)$ is equivalent to having u “success” in u Bernoulli trials, each of which has a success probability $1 - \exp(-t_s/t_c)$:

$$f(u, v) = \binom{u}{v} (1 - \exp(-t_s/t_c))^v \exp(-(u - v)t_s/t_c). \quad (20)$$

With (19) and (20) respectively capturing the dynamics of EV arrival and battery circulation, we can proceed to establish the queueing equilibrium. The system can be characterized by a state tuple (i, j) representing that there are i EVs (including those waiting and being served) and j fully-charged batteries in the station. Denote $G_t(i, j)$ as the probability of system state (i, j) at time t and denote $G_{t+t_s}(\hat{i}, \hat{j})$ as the probability of system state (\hat{i}, \hat{j}) at time $t + t_s$. We can then compute $G_{t+t_s}(\hat{i}, \hat{j})$ given $G_t(i, j)$:

$$G_{t+t_s}(\hat{i}, \hat{j}) = \begin{cases} \sum_{i=0}^K \sum_{j=0}^B G_t(i, j) g(\hat{i} - i + \Delta) f(B - j, \hat{j} - j + \Delta), & \hat{i} < K, \\ \sum_{i=0}^K \sum_{j=0}^B G_t(i, j) \left(1 - \sum_{d=1}^{K-1} g(d - i + \Delta) \right) f(B - j, \hat{j} - j + \Delta), & \hat{i} = K, \end{cases} \quad (21a)$$

$$\left(1 - \sum_{d=1}^{K-1} g(d - i + \Delta) \right) f(B - j, \hat{j} - j + \Delta), \quad \hat{i} = K, \quad (21b)$$

where $\Delta = \min\{i, j, S\}$ is the number of EVs leaving the station with fully-charged batteries during $(t, t + t_s]$. When the queue is not full at $t + t_s$, i.e., $\hat{i} < K$, the transition from (i, j) to (\hat{i}, \hat{j}) is equivalent to having $\hat{i} - i + \Delta$ EVs arriving and $\hat{j} - j + \Delta$ batteries finishing charging. However, if the queue capacity is reached, i.e., $\hat{i} = K$, there are at least $K - i - \Delta$ new arrivals during $(t, t + t_s]$, which happens with a probability of $1 - \sum_{d=1}^{K-1} g(d - i + \Delta)$. The equilibrium state distribution, denoted as $G(i, j) = \lim_{t \rightarrow \infty} G_t(i, j)$, is given by solving (21) together with the normalization equation $\sum_{i=0}^K \sum_{j=0}^B G(i, j) = 1$. Note that the equation system consists of $(K + 1) \times (B + 1) + 1$ linear equations but only $(K + 1) \times (B + 1)$ variables, which may not necessarily have a unique solution. Whereas it is proven in [63, Theorem 1] that the corresponding embedded Markov chain is ergodic. Thereby we can always find a unique equilibrium state distribution $G(i, j)$, based on which we can derive the average waiting time $w_{i,t}^s$. An efficient approach to computing

$G(i, j)$ without solving an equation system is detailed in [Appendix B](#). The expected queue length is $L = \sum_{i=0}^W \sum_{j=0}^B i \cdot G(i, j)$. Applying the Little's law yields

$$L_s = \bar{\lambda}_{i,t}^s (w_{i,t}^s + t_s) \left(1 - \sum_{j=0}^B G(K, j) \right), \quad (22)$$

where $1 - \sum_{j=0}^B G(K, j)$ represents the probability that the queue is not full. Hence, the average waiting time at battery swapping stations is given by

$$w_{i,t}^s = \frac{\sum_{i=0}^K \sum_{j=0}^B i \cdot G(i, j)}{\bar{\lambda}_{i,t}^s \left(1 - \sum_{j=0}^B G(K, j) \right)} - t_s. \quad (23)$$

In this study, charging and battery swapping queues are both considered finite. As a result, an EV would have to seek an alternative location and mode for recharging if the queue is full upon its arrival. However, it is important to note that we assume a large queue capacity in this study to prevent the case of a full queue. This consideration is based on the observation that drivers do not necessarily wait exactly at the stations, as these stations might have limited space to accommodate a long queue. Instead, drivers can wait in the vicinity of the charging facilities, such as roadside parking spaces or nearby parking lots, where a significantly larger number of vehicles can be held in queue. With a large queue capacity, the blocking rate is negligible for any EV arrival rate in a practical range. We show in [Appendix C](#) that the blocking rate becomes nonnegligible only when demand at each station is very high. In this case, the waiting time is prohibitively long, which deters EVs from using the facility at equilibrium. To avoid this, we further enforce the following constraint:

$$0 \leq \lambda_{i,t}^k \leq \rho_k x_{i,t}^k, \quad (24)$$

which imposes an upper bound ρ_k on the average arrival rate of each facility. This ensures the actual charging demand falls in a reasonable regime where the consequent waiting time remains tolerable (e.g., less than 1 hour) and the blocking rate remains marginal. From this perspective, constraint (24) can be interpreted as a quality of service (QoS) guarantee for the infrastructure network.³

Remark 2. *In situations where the queue capacity is small, the probability of blocking may become non-negligible, and the model has to be revised accordingly. One potential approach to address this concern is to consider a slightly different queuing model, where there are multiple charging stations from the same zone in each queue, and the driver would choose which station to approach within the same zone based on which station has the shortest queuing time. In this case, the blocking probability could be negligible, as the likelihood of all charging stations in the same zone being fully occupied is quite low. In this paper, we focus on the large capacity case and leave the other case as future work.*

3.6. Decision-Making Problem

The decision-making process in this study involves both the platform and EV drivers. The platform makes planning decisions ($x_{i,t}^k$) and operational decisions ($q_{ij,t}, r_{ij,t}, N_{i,t}^v$), based on which EV drivers decide their charging locations and modes through $f_{ij,t}^k$. These decisions not only influence endogenous variables such as $\Lambda_{i,t}$, $\lambda_{i,t}^k$, and $w_{i,t}^k$ but also determine the fleet size:

$$N_t = \sum_{i \in \mathcal{I}} N_{i,t}^v + \sum_{i \in \mathcal{I}} \sum_{j \in \mathcal{I}} q_{ij,t} w_{i,t}^p + \sum_{i \in \mathcal{I}} \sum_{j \in \mathcal{I}} q_{ij,t} t_{ij} + \sum_{i \in \mathcal{I}} \sum_{j \in \mathcal{I}} r_{ij,t} t_{ij} + \sum_{i \in \mathcal{I}} \sum_{j \in \mathcal{I}} \sum_{k \in \mathcal{K}} f_{ij,t}^k t_{ij} + \sum_{i \in \mathcal{I}} \sum_{k \in \mathcal{K}} \lambda_{i,t}^k (w_{i,t}^k + t_k) \quad (25)$$

³Results in our case studies demonstrate that this constraint is always inactive, indicating that EV drivers will strategically avoid congested facilities with high chance of blockage.

where the first four terms represent EVs in operations, while the last two terms account for the total number of EVs traveling to, waiting at, and being served in charging and battery swapping stations. The platform's revenue at each stage from ride-hailing services can be then represented as

$$\Pi_t^r = \sum_{i \in \mathcal{I}} \sum_{j \in \mathcal{I}} p_{ij,t} q_{ij,t} - \gamma_e N_t - \gamma_p \sum_{i \in \mathcal{I}} \sum_{j \in \mathcal{I}} \sum_{k \in \mathcal{K}} f_{ij,t}^k u_{i,t}, \quad (26)$$

where γ_e is the unit cost of each EV and γ_p is a penalty parameter. The last term penalizes the total time cost resulting from drivers' charging behaviors, which ensures that charging infrastructure is properly deployed to maintain charging costs within an acceptable range. On the other hand, the deployment cost of charging facilities at each stage is

$$\Pi_t^c = \sum_{i \in \mathcal{I}} \sum_{k \in \mathcal{K}} \gamma_k (x_{i,t}^k - x_{i,t-1}^k). \quad (27)$$

The platform stops building charging infrastructure after stage T . However, the infrastructure will stay and remain functional beyond time T until it exceeds the lifespan, i.e., $H > T$. Therefore, the deployment cost is incurred in the first T stages, while the platform's revenue and operational costs remain unchanged from stage $T + 1$ onward until H . To reflect the preference for immediate costs or benefits over future ones and accounts for the time value of money and/or risk, we introduce a discount factor $\gamma \in (0, 1)$ [64]. The total profit over the entire operation horizon is then defined as

$$\Pi = \sum_{t \in \mathcal{T}} \gamma^{t-1} (\Pi_t^r - \Pi_t^c) + \frac{\gamma^T - \gamma^H}{1 - \gamma} \Pi_T^r. \quad (28)$$

By equivalently replacing the driver's decision problem with equilibrium conditions (14), we formulate the decision-making problem as a mathematical program with complementarity constraints (MPCC):

$$\underset{x, q, r, f, u, N^v}{\text{maximize}} \quad \sum_{t \in \mathcal{T}} \gamma^{t-1} (\Pi_t^r - \Pi_t^c) + \frac{\gamma^T - \gamma^H}{1 - \gamma} \Pi_T^r \quad (29a)$$

subject to constraints (1) – (25)

$$N_{i,t}^v > \hat{N}^v, \quad \forall t \in \mathcal{T}, i \in \mathcal{I}, \quad (29b)$$

$$q_{ij,t} > 0, \quad \forall t \in \mathcal{T}, i \in \mathcal{I}, j \in \mathcal{I} \quad (29c)$$

$$x_{i,0}^k \leq x_{i,t}^k \leq \hat{x}_i^k, \quad \forall t \in \mathcal{T}, i \in \mathcal{I}, k \in \mathcal{K}, \quad (29d)$$

where \hat{N}^v is the lower bound for the number of idle vehicle in each zone, which reflects the practice that the platform will maintain the vehicle supply above a certain threshold to ensure service quality; and \hat{x}_i^k is the maximum number of facilities allowed to deploy in each zone because of practical restrictions, e.g., limited land supply. This optimization problem is inherently challenging to solve due to the complementarity constraints (14) and the nonconvex constraints (8)(18)(23).

4. Solution Method

In this section, we will present our approach for pinpointing stationary points for (29) and subsequently establish a theoretical upper bound based on model relaxation and decomposition.

4.1. Finding Stationary Points

Nonlinear programming methods typically require constraint qualification to ensure the existence and boundedness of Lagrange multipliers and the satisfaction of Karush-Kuhn-Tucker (KKT) conditions.

The complementarity constraints (14), however, violate Mangasarian-Fromovitz Constraint Qualification (MFCQ) at any feasible point because of their combinatorial nature. Therefore, directly solving (29) using common nonlinear programming algorithms may not be able to obtain a local stationary point.

To address this issue, an auxiliary parameter ϵ is introduced to relax the complementarity condition (14c):

$$f_{ij,t}^k(c_{ij,t}^k - u_{i,t}) \leq \epsilon, \quad (30)$$

which is a common relaxation scheme to iteratively compute the stationary point of MPCC [65][66][67]. For any $\epsilon > 0$, the gradients of active constraints are linear independent. Therefore, the resulting optimization problem satisfies constraint qualification and can be solved using nonlinear programming algorithms. We can start from a relatively large value of ϵ and gradually decrease its value. At each iteration, we solve the corresponding optimization problem using the solution obtained from the previous iteration as an initial guess. The iterative process terminates at a sufficiently small ϵ , where we obtain a solution that can be used to derive an exact solution to the original problem (29).

4.2. Derivation of Upper Bounds

Nonlinear programming algorithms, although capable of finding local solutions, do not provide any performance guarantee. To address this limitation, our objective is to establish an upper bound for the original problem, which will enable us to verify the optimality of any obtained solution, even in the absence of concavity. However, it is important to note that finding a tight upper bound for nonconcave optimization problems is a challenging task due to the complexity and diversity of problem structures. Common approaches to establishing upper bounds heavily rely on relaxation techniques, such as convex relaxation and linear programming relaxation, which results in a simplified optimization problem that is easier to solve. In the same vein, we leverage the problem's characteristics and propose a relaxed formulation that presents favorable structures while preserving the essence of the original problem, based on which a high-quality upper bound can be found.

4.2.1. Model Relaxation

The original formulation is relaxed by assuming that the platform has direct control over the actual charging demand $\lambda_{i,t}^k$ in each zone by regulating vehicle flow $f_{ij,t}^k$. However, charging mode choice is still subject to equilibrium conditions, meaning that EV drivers only decide their charging modes within the zone assigned by the platform. This relaxation is grounded in the intuition that the actual charging demand is naturally close to the desired pattern of the platform, since the platform can induce the desired charging behavior through planning and operational decisions. Furthermore, the preferred charging patterns of drivers and the platform are partially aligned because of their mutual objective of reducing the charging cost. Given these considerations, we believe this relaxation will not result in a significant deviation.

After the relaxation, we can replace $f_{ij,t}^k$ with $\lambda_{i,t}^k$ in the formulation. Define the relaxed charging cost as:

$$\tilde{c}_{i,t}^k = \tilde{t}_i + w_{i,t}^k + t_k, \quad (31)$$

in which $\tilde{t}_i = \min_{\forall j} \{t_{ji}\}$ denotes the minimum time required to reach zone i . The equilibrium condition for charging mode choice then becomes:

$$\begin{cases} \lambda_{i,t}^k \geq 0, & (32a) \\ \tilde{c}_{i,t}^k - \tilde{u}_{i,t} \geq 0, & (32b) \\ \lambda_{i,t}^k (\tilde{c}_{i,t}^k - \tilde{u}_{i,t}) = 0, & (32c) \end{cases}$$

where $\tilde{u}_{i,t}$ is the resulting equilibrium charging cost. By definition, we further have $\tilde{c}_{i,t}^k \leq c_{j,i,t}^k$ and $\tilde{u}_{i,t} \leq u_{i,t}$. Consequently, the total charging cost can be expressed as:

$$\sum_{i \in \mathcal{I}} \sum_{k \in \mathcal{K}} \lambda_{i,t}^k \tilde{u}_{i,t} = \sum_{i \in \mathcal{I}} \sum_{j \in \mathcal{I}} \sum_{k \in \mathcal{K}} f_{ij,t}^k \tilde{c}_{j,t}^k \leq \sum_{i \in \mathcal{I}} \sum_{j \in \mathcal{I}} \sum_{k \in \mathcal{K}} f_{ij,t}^k c_{ij,t}^k = \sum_{i \in \mathcal{I}} \sum_{j \in \mathcal{I}} \sum_{k \in \mathcal{K}} f_{ij,t}^k u_{i,t}, \quad (33)$$

which is upper bounded by the original one. By replacing t_{ij} in the second last term of (25) with \tilde{t}_i , we can also relax the fleet size to be

$$\begin{aligned} \tilde{N}_t &= \sum_{i \in \mathcal{I}} N_{i,t}^v + \sum_{i \in \mathcal{I}} \sum_{j \in \mathcal{I}} q_{ij,t} w_{i,t}^p + \sum_{i \in \mathcal{I}} \sum_{j \in \mathcal{I}} q_{ij,t} t_{ij} + \sum_{i \in \mathcal{I}} \sum_{j \in \mathcal{I}} r_{ij,t} t_{ij} + \sum_{i \in \mathcal{I}} \sum_{j \in \mathcal{I}} \sum_{k \in \mathcal{K}} f_{ij,t}^k \tilde{t}_j + \sum_{i \in \mathcal{I}} \sum_{k \in \mathcal{K}} \lambda_{i,t}^k (w_{i,t}^k + t_k) \\ &= \sum_{i \in \mathcal{I}} N_{i,t}^v + \sum_{i \in \mathcal{I}} \sum_{j \in \mathcal{I}} q_{ij,t} w_{i,t}^p + \sum_{i \in \mathcal{I}} \sum_{j \in \mathcal{I}} q_{ij,t} t_{ij} + \sum_{i \in \mathcal{I}} \sum_{j \in \mathcal{I}} r_{ij,t} t_{ij} + \sum_{i \in \mathcal{I}} \sum_{k \in \mathcal{K}} \lambda_{i,t}^k (\tilde{t}_i + w_{i,t}^k + t_k). \end{aligned} \quad (34)$$

Correspondingly, the energy balance condition (11) becomes

$$\sum_{i \in \mathcal{I}} N_{i,t}^v + \sum_{i \in \mathcal{I}} \sum_{j \in \mathcal{I}} q_{ij,t} w_{i,t}^p + \sum_{i \in \mathcal{I}} \sum_{j \in \mathcal{I}} q_{ij,t} t_{ij} + \sum_{i \in \mathcal{I}} \sum_{j \in \mathcal{I}} r_{ij,t} t_{ij} = \sum_{i \in \mathcal{I}} \sum_{k \in \mathcal{K}} \lambda_{i,t}^k \left[\frac{(1-\varepsilon)\Omega}{\omega} - \tilde{t}_i \right]. \quad (35)$$

For notation brevity, we further rewrite the coefficients in (29a) as $\sigma_t^c = \gamma^{t-1}$ and

$$\sigma_t^r = \begin{cases} \gamma^{t-1}, & t < T, \\ \frac{\gamma^{T-1} - \gamma^H}{1 - \gamma}, & t = T. \end{cases} \quad (36a)$$

$$\sigma_t^r = \begin{cases} \gamma^{t-1}, & t < T, \\ \frac{\gamma^{T-1} - \gamma^H}{1 - \gamma}, & t = T. \end{cases} \quad (36b)$$

After these modifications, the original problem (29) is reformulated as follows:

$$\underset{x, q, r, \lambda, \tilde{u}, N^v}{\text{maximize}} \quad \sum_{t \in \mathcal{T}} (\sigma_t^r \Pi_t^r - \sigma_t^c \Pi_t^c) \quad (37a)$$

$$\text{subject to} \quad \sum_{i \in \mathcal{I}} \sum_{k \in \mathcal{K}} \gamma_k x_{i,t}^k \leq b_t, \quad \forall t \in \mathcal{T}, \quad (37b)$$

$$N_{i,t}^v > \hat{N}^v, \quad \forall t \in \mathcal{T}, i \in \mathcal{I}, \quad (37c)$$

$$q_{ij,t} > 0, \quad \forall t \in \mathcal{T}, i \in \mathcal{I}, j \in \mathcal{I}, \quad (37d)$$

$$x_{i,0}^k \leq x_{i,t}^k \leq \hat{x}_i^k, \quad \forall t \in \mathcal{T}, i \in \mathcal{I}, k \in \mathcal{K}, \quad (37e)$$

$$x_{i,t}^k - x_{i,t-1}^k \geq 0, \quad \forall t \in \mathcal{T}, i \in \mathcal{I}, k \in \mathcal{K}, \quad (37f)$$

$$0 \leq \lambda_{i,t}^k \leq \rho_k x_{i,t}^k, \quad \forall t \in \mathcal{T}, i \in \mathcal{I}, k \in \mathcal{K}, \quad (37g)$$

$$\lambda_{i,t}^k (\tilde{c}_{i,t}^k - \tilde{u}_{i,t}) \leq \epsilon, \quad \forall t \in \mathcal{T}, i \in \mathcal{I}, k \in \mathcal{K}, \quad (37h)$$

$$\tilde{c}_{i,t}^k - \tilde{u}_{i,t} \geq 0, \lambda_{i,t}^k \geq 0, \quad \forall t \in \mathcal{T}, i \in \mathcal{I}, k \in \mathcal{K}, \quad (37i)$$

$$\sum_{j \in \mathcal{I}} (q_{ij,t} + r_{ij,t}) = \sum_{j \in \mathcal{I}} (q_{ji,t} + r_{ji,t}), \quad \forall t \in \mathcal{T}, i \in \mathcal{I}, \quad (37j)$$

$$\sum_{i \in \mathcal{I}} N_{i,t}^v + \sum_{i \in \mathcal{I}} \sum_{j \in \mathcal{I}} (q_{ij,t} w_{i,t}^p + q_{ij,t} t_{ij} + r_{ij,t} t_{ij}) = \sum_{i \in \mathcal{I}} \sum_{k \in \mathcal{K}} \lambda_{i,t}^k \left[\frac{(1-\varepsilon)\Omega}{\omega} - \tilde{t}_i \right], \quad \forall t \in \mathcal{T}. \quad (37k)$$

Compared to (29), the relaxed problem (37) remains nonconcave but is more tractable owing to its decomposable structure, which can be leveraged to derive an upper bound subsequently.

4.2.2. Model Decomposition

The derivation of upper bounds is based on Lagrangian relaxation, whose performance is sensitive to the quality of Lagrange multipliers. Therefore, constraint (37f) is removed from (37) and the complementarity

constraint (37h) is relaxed by ϵ as in (30). These modifications effectively improve the tractability of (37) without compromising the validity of model relaxation. Let $\Phi = (\eta, \mu, \theta)$ be the Lagrange multipliers associated with (37b), (37j), and (37k), respectively. The partial Lagrangian is:

$$\begin{aligned} \mathcal{L}(x, q, r, \lambda, \tilde{u}, N^v) \Big|_{\Phi} &= \sum_{t \in \mathcal{T}} (\sigma_t^r \Pi_t^r - \sigma_t^c \Pi_t^c) + \sum_{t \in \mathcal{T}} \sum_{i \in \mathcal{I}} \sum_{j \in \mathcal{I}} (\mu_{i,t} - \mu_{j,t}) (q_{ij,t} + r_{ij,t}) \\ &\quad - \sum_{t \in \mathcal{T}} \sum_{i \in \mathcal{I}} \sum_{k \in \mathcal{K}} \eta_t \gamma_k x_{i,t}^k + \sum_{t \in \mathcal{T}} \sum_{i \in \mathcal{I}} \theta_t N_{i,t}^v + \sum_{t \in \mathcal{T}} \sum_{i \in \mathcal{I}} \sum_{j \in \mathcal{I}} \theta_t q_{ij,t} w_{i,t}^p \\ &\quad + \sum_{t \in \mathcal{T}} \sum_{i \in \mathcal{I}} \sum_{j \in \mathcal{I}} \theta_t (q_{ij,t} + r_{ij,t}) t_{ij} - \sum_{t \in \mathcal{T}} \sum_{i \in \mathcal{I}} \sum_{k \in \mathcal{K}} \theta_t \lambda_{i,t}^k \left[\frac{(1-\epsilon)\Omega}{\omega} - \tilde{t}_i \right] \end{aligned} \quad (38)$$

Since $w_{i,t}^k$ only depends on $x_{i,t}^k$ and $\lambda_{i,t}^k$, given the multipliers, the Lagrangian is separable in both spatial and temporal dimensions, i.e., $\mathcal{L}(x, q, r, \lambda, \tilde{u}, N^v) = \sum_{t \in \mathcal{T}} \sum_{i \in \mathcal{I}} \mathcal{L}_{i,t}(x_{i,t}^k, q_{ij,t}, r_{ij,t}, \lambda_{i,t}^k, \tilde{u}_{i,t}, N_{i,t}^v)$, where

$$\begin{aligned} \mathcal{L}_{i,t}(x_{i,t}^k, q_{ij,t}, r_{ij,t}, \lambda_{i,t}^k, \tilde{u}_{i,t}, N_{i,t}^v) \Big|_{\Phi} &= \sigma_t^r \sum_{j \in \mathcal{I}} p_{ij,t} q_{ij,t} - (\sigma_t^c - \sigma_{t+1}^c + \eta_t) \sum_{k \in \mathcal{K}} \gamma_k x_{i,t}^k - \sigma_t^r (\gamma_e + \gamma_p) \sum_{k \in \mathcal{K}} \lambda_{i,t}^k \tilde{u}_{i,t} \\ &\quad + (\theta_t - \sigma_t^r \gamma_e) N_{i,t}^v + (\theta_t - \sigma_t^r \gamma_e) \sum_{j \in \mathcal{I}} (q_{ij,t} w_{i,t}^p + q_{ij,t} t_{ij} + r_{ij,t} t_{ij}) \\ &\quad + \sum_{j \in \mathcal{I}} (\mu_{i,t} - \mu_{j,t}) (q_{ij,t} + r_{ij,t}) - \theta_t \sum_{k \in \mathcal{K}} \lambda_{i,t}^k \left[\frac{(1-\epsilon)\Omega}{\omega} - \tilde{t}_i \right]. \end{aligned} \quad (39)$$

Note that $\sigma_t^c = 0$ if $t > T$. Therefore, we can separately optimize a subproblem for zone i and stage t :

$$\text{maximize} \quad \mathcal{L}_{i,t}(x_{i,t}^k, q_{ij,t}, r_{ij,t}, \lambda_{i,t}^k, \tilde{u}_{i,t}, N_{i,t}^v) \Big|_{\Phi} \quad (40a)$$

$$\text{subject to} \quad N_{i,t}^v > \hat{N}^v, \quad (40b)$$

$$q_{ij,t} > 0, \quad \forall j \in \mathcal{I}, \quad (40c)$$

$$x_{i,0}^k \leq x_{i,t}^k \leq \hat{x}_i^k, \quad \forall k \in \mathcal{K}, \quad (40d)$$

$$0 \leq \lambda_{i,t}^k \leq \rho_k x_{i,t}^k, \quad \forall k \in \mathcal{K}, \quad (40e)$$

$$\lambda_{i,t}^k (\tilde{c}_{i,t}^k - \tilde{u}_{i,t}) \leq \epsilon, \quad \forall k \in \mathcal{K}, \quad (40f)$$

$$\tilde{c}_{i,t}^k - \tilde{u}_{i,t} \geq 0, \lambda_{i,t}^k \geq 0, \quad \forall k \in \mathcal{K}. \quad (40g)$$

However, finding the global optimum for each subproblem remains challenging due to their nonconcave nature. Fortunately, we observe that each subproblem (40) can be further divided into two smaller-scale subproblems that are easier to solve.

The first one is an optimization over $N_{i,t}^v, q_{ij,t}$, and $r_{ij,t}, \forall j \in \mathcal{I}$:

$$\begin{aligned} \text{maximize}_{N_{i,t}^v, q_{ij,t}, r_{ij,t}} \quad & \sigma_t^r \sum_{j \in \mathcal{I}} p_{ij,t} q_{ij,t} + (\theta_t - \sigma_t^r \gamma_e) \sum_{j \in \mathcal{I}} (q_{ij,t} w_{i,t}^p + q_{ij,t} t_{ij} + r_{ij,t} t_{ij}) \\ & + (\theta_t - \sigma_t^r \gamma_e) N_{i,t}^v + \sum_{j \in \mathcal{I}} (\mu_{i,t} - \mu_{j,t}) (q_{ij,t} + r_{ij,t}) \end{aligned} \quad (41)$$

$$\text{subject to} \quad N_{i,t}^v \geq \hat{N}^v,$$

$$q_{ij,t} > 0, r_{ij,t} \geq 0, \quad \forall j \in \mathcal{I}.$$

Recall that the revenue term is concave with respect to passenger demand $q_{ij,t}$ for most commonly used demand functions (e.g, logit model, linear demand function, exponential demand function, etc). Therefore,

given any fixed $N_{i,t}^v$, passenger waiting time is uniquely determined by (4), and the above problem becomes a concave program over $q_{ij,t}$ and $r_{ij,t}$, allowing us to find the optimal values of $q_{ij,t}$ and $r_{ij,t}$ corresponding to different values of $N_{i,t}^v$. We can therefore optimally solve (41) by searching over a one-dimensional space of $N_{i,t}^v$.

The second subproblem is a nonconcave optimization over $\tilde{u}_{i,t}$, $x_{i,t}^k$ and $\lambda_{i,t}^k, \forall k \in \mathcal{K}$:

$$\begin{aligned}
& \underset{x_{i,t}^k, \lambda_{i,t}^k, \tilde{u}_{i,t}}{\text{maximize}} && -(\sigma_t^c - \sigma_{t+1}^c + \eta_t) \sum_{k \in \mathcal{K}} \gamma_k x_{i,t}^k - \sigma_t^r (\gamma_e + \gamma_p) \sum_{k \in \mathcal{K}} \lambda_{i,t}^k \tilde{u}_{i,t} - \theta_t \sum_{k \in \mathcal{K}} \lambda_{i,t}^k \left[\frac{(1-\varepsilon)\Omega}{\omega} - \tilde{t}_i \right] \\
& \text{subject to} && x_{i,0}^k \leq x_{i,t}^k \leq \bar{x}_i^k, \quad \forall k, \\
& && 0 \leq \lambda_{i,t}^k \leq \rho_k x_{i,t}^k, \quad \forall k, \\
& && \lambda_{i,t}^k (\tilde{c}_{i,t}^k - \tilde{u}_{i,t}) \leq \epsilon, \quad \forall k, \\
& && \tilde{c}_{i,t}^k - \tilde{u}_{i,t} \geq 0, \lambda_{i,t}^k \geq 0, \quad \forall k.
\end{aligned} \tag{42}$$

Given that the set \mathcal{K} is two-dimensional, this subproblem has a decision space of five dimensions. Despite its nonconcavity, we can proceed by adopting a hierarchical approach where we first fix $\tilde{u}_{i,t}$ and then solve the two residual problems over $(x_{i,t}^k, \lambda_{i,t}^k)$ for different k . Note that these two residual problems are independent and each one is two-dimensional with a closed and bounded decision space. Therefore, through the proposed hierarchical approach, the computational cost of (42) is equivalent to two three-dimensional optimization problems, which can be efficiently solved using brute-force enumeration without requiring the problem to be concave. Overall, we divide the subproblem into (41) and (42), each of which has favorable properties (concavity for (41) and low-dimensionality for (42)) and can be solved using a hierarchical approach. Consequently, we can optimally solve each subproblem (40).

Based on the weak duality theorem, for any given Lagrange multipliers η, μ, θ , the solutions to all subproblems collectively provide a valid upper bound for the relaxed problem (37). This bound can be further improved by iteratively updating Lagrange multipliers within a dual decomposition framework as follows:

$$\left\{ \begin{aligned}
& \eta_t \leftarrow \max \left\{ 0, \eta_t - \zeta \left(b_t - \sum_{i \in \mathcal{I}} \sum_{k \in \mathcal{K}} \gamma_k x_{i,t}^k \right) \right\}, & (43a) \\
& \mu_{i,t} \leftarrow \mu_{i,t} - \zeta \left(\sum_{j \in \mathcal{I}} (q_{ij,t} + r_{ij,t}) - \sum_{j \in \mathcal{I}} (q_{ji,t} + r_{ji,t}) \right), & (43b) \\
& \theta_t \leftarrow \theta_t - \zeta \left[\sum_{i \in \mathcal{I}} N_{i,t}^v + \sum_{i \in \mathcal{I}} \sum_{j \in \mathcal{I}} (q_{ij,t} w_{i,t}^p + q_{ij,t} t_{ij} + r_{ij,t} t_{ij}) - \sum_{i \in \mathcal{I}} \sum_{k \in \mathcal{K}} \lambda_{i,t}^k \left(\frac{(1-\varepsilon)\Omega}{\omega} - \tilde{t}_i \right) \right], & (43c)
\end{aligned} \right.$$

where ζ is the step size. Due to the model relaxation, the established upper bound is an overestimation of the globally optimal solution to the original problem (29). In other words, the bound is also a theoretical upper bound for the original problem, which allows us to quantify the optimality of its solution. We summarize the derivation procedure as follows:

- **Step 1:** Solve the original problem (29) via nonlinear programming solvers. The solution provides a valid lower bound for (29).
- **Step 2:** Solve the relaxed problem (37) via nonlinear programming solvers and obtain the corresponding Lagrange multipliers (η, μ, θ) .
- **Step 3:** Plug (η, μ, θ) into (40). Find the globally optimal solution to each subproblem by solving (41) and (42), respectively.

- **Step 4:** Combine subproblems’ solutions to establish a valid upper bound for (29). Evaluate the bound performance by measuring the gap between lower and upper bounds.
- **Step 5:** Terminate the procedure if the optimality gap is satisfactorily tight. Otherwise, update the multipliers according to (43) and go to **Step 3**.

The aforementioned procedure can be terminated at any iteration, and regardless of when it is terminated, the derived bound is always a valid upper bound for the original problem [68]. The proposed algorithm is an example of how the problem’s unique structure can be leveraged to assess the solution optimality of a highly nonconcave optimization problem after proper model relaxations, given that a feasible solution can be derived by some other gradient-based nonlinear programming solvers. We emphasize that the proposed method is nontrivial and rather useful. Because for most large-scale nonconcave problems, it may not be challenging to find a local solution using nonlinear programming solvers, but it is significantly difficult to examine how good the solution is compared to the unknown globally optimal one. In this work, we tackle this intrinsic challenge by relaxing the original problem to another nonconcave problem with decomposable structures. By leveraging the problem’s favorable properties, we show that each subproblem can be optimally solved even in the presence of nonconcavity, thereby allowing us to evaluate the distance between the obtained solution and the globally optimal one.

5. Numerical Studies

Based on the proposed formulation and analytical analysis, this section presents several case studies to validate the solution optimality and discuss the effectiveness of the joint deployment scheme.

5.1. Simulation Settings

A series of case studies are conducted for Manhattan, New York City, where a platform jointly deploys charging infrastructure and operates a ride-hailing fleet. The island is divided into 20 zones.⁴ Real data from the New York City Taxi and Limousine Commission (NYCTLC) [69] was used to estimate travel demand \bar{q}_{ij} , including pickup and dropoff locations as well as trip duration. An exponential function is utilized as the demand model in (3):

$$q_{ij,t} = \bar{q}_{ij} \exp\left(-\alpha(p_{ij,t} + \beta w_{i,t}^p)\right), \quad (44)$$

where $\alpha > 0$ is a sensitivity parameter. We consider a three-stage infrastructure investment plan, i.e., $T = 3$. To capture the entire expansion process of an infrastructure network, we define $x_{i,0}^k = 0, \forall i \in \mathcal{I}, k \in \mathcal{K}$, implying that there is no charging facility before the first planning stage. Parameters related to EVs and infrastructure are calibrated to align with industry practices. Particularly, we assume all charging and battery swapping stations share the same configuration to ensure a fair comparison. For ease of comprehension, the number of swapping stations is used to quantify the total budget. On the other hand, parameters related to ride-hailing operations are calibrated via reverse engineering with partial reference to [57] such that the proposed model reproduces an equilibrium solution that is close to empirical data. The detailed parameter settings are summarized and justified in Appendix A. In Steps 1 and 2 of our proposed solution procedure, we adopt the interior-point algorithm implemented in `fmincon` to obtain local solutions and Lagrange multipliers. Numerical simulations in this study are conducted on a desktop computer equipped with an Intel 8-core i7-9700 CPU.

⁴The proposed model and solution framework are theoretically applicable to real-world networks with many more zones. But a 20-zone model should suffice to show the efficacy of our methodology.

5.2. Solution Optimality

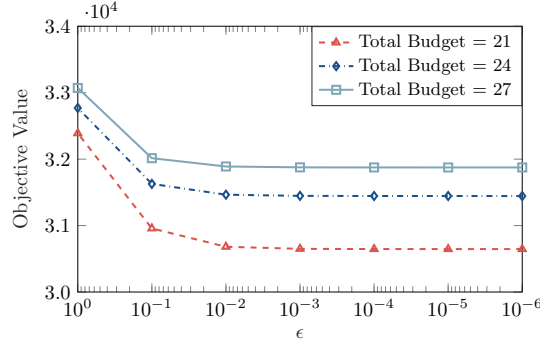


Figure 2: Objective value under different values of relaxation parameter ϵ .

As mentioned in 4.1, a stationary point of the joint planning problem (29) can be found by iteratively reducing the relaxation parameter ϵ . As shown in Figure 2, we can obtain a local solution under different settings, which serves as a lower bound for (29). While an upper bound can be established using the proposed relaxation and decomposition approach. The solution optimality is comprehensively evaluated across various budget levels, parameter settings, and network sizes. A six-zone network is included as it will be used in the subsequent section to visualize the expansion process of infrastructure networks. To benchmark the established upper bound, we derive another upper bound by applying Lagrangian relaxation on the original problem, where the complementarity constraint is linearized using the big-M method to enable decomposition. The derivation of this benchmark upper bound is detailed in Appendix D.

Table 1: Solution optimality under different simulation settings.

γ	γ_p	Totl. Budget	# of Zones	LB ($\times 10^4$)	BM UB ($\times 10^4$)	BM Gap	Our UB ($\times 10^4$)	Our Gap	Totl.Time (min)
0.90	20	21	20	2.992	17.171	82.57%	3.088	3.11%	99.63
0.90	20	24	20	3.045	16.965	82.05%	3.125	2.56%	104.12
0.90	20	27	20	3.071	15.100	79.66%	3.156	2.71%	100.25
0.85	20	21	20	2.608	15.172	82.81%	2.693	3.15%	95.04
0.85	20	24	20	2.652	15.262	82.62%	2.725	2.68%	96.03
0.85	20	27	20	2.673	13.589	80.33%	2.755	2.97%	94.72
0.95	20	21	20	3.435	18.453	81.39%	3.543	3.07%	99.88
0.95	20	24	20	3.498	18.129	80.70%	3.589	2.52%	99.79
0.95	20	27	20	3.531	16.891	79.10%	3.620	2.48%	99.03
0.90	15	21	20	3.066	15.102	79.70%	3.164	3.09%	92.51
0.90	15	24	20	3.117	14.615	78.67%	3.191	2.33%	99.58
0.90	15	27	20	3.132	13.348	76.54%	3.218	2.69%	93.62
0.90	25	21	20	2.921	18.385	84.11%	3.021	3.31%	102.86
0.90	25	24	20	2.976	18.233	83.68%	3.063	2.85%	101.97
0.90	25	27	20	3.012	17.219	82.51%	3.097	2.74%	98.75
0.90	20	21	6	3.065	27.091	88.69%	3.193	4.03%	34.88
0.90	20	24	6	3.145	29.496	89.34%	3.233	2.72%	35.72
0.90	20	27	6	3.188	30.777	89.64%	3.263	2.33%	36.91

Table 1 reports the optimality gap and the computation time of Step 3 after one iteration, which is the most time-consuming component in the proposed method. The results demonstrate the consistent performance

of our approach across different settings. Using the multipliers obtained in Step 2 without further updates, we can achieve a tight upper bound with an optimality gap of approximately 3%, indicating that a near-optimal solution to (29) is attained. In contrast, the benchmark method cannot provide an accurate estimation of the unknown globally optimal solution. A major reason is that in the benchmark approach, the complementarity constraint has to be first linearized using the big-M method and then dualized to ensure decomposability. However, this process introduces strong linearity in the relaxed problem, which tends to produce extreme solutions that compromise the quality of the derived bound. As a result, the Lagrangian relaxation in the benchmark approach only yields a trivial upper bound with up to 80% optimality gap, providing little insight into the problem’s true complexity. Our proposed method, however, circumvents the need to dualize the complementarity constraint by employing appropriate relaxations based on the inherent characteristics of the problem. By doing so, we simplify the complex model into a more tractable form with favorable structures, while still capturing the essential features of the problem. Importantly, the complementarity constraint remains respected in the relaxed subproblem, allowing us to derive a significantly tighter upper bound compared to the benchmark approach. Besides, the average computation time to optimally solve each subproblem in the proposed method is less than 2 minutes. We emphasize that this solving time is satisfactorily short for an infrastructure planning problem that does not require real-time computation. In fact, the computation time is orders of magnitude shorter than the implementation time of a deployment plan (e.g., in the range of months or years), rendering it insignificant for the planning purpose. This comprehensive evaluation confirms the effectiveness and efficiency of our proposed approach.

5.3. Synergy between Charging and Battery Swapping

To assess the performance of joint planning, we vary the total budget and compare different deployment strategies, including jointly deploying charging and battery swapping facilities versus deploying only one of them. The total profit obtained from each strategy is shown in Figure 3a, and the corresponding average charging cost, defined as

$$\bar{c} = \frac{\sum_{t \in \mathcal{T}} \sum_{i \in \mathcal{I}} \sum_{j \in \mathcal{I}} \sum_{k \in \mathcal{K}} f_{ij,t}^k u_{i,t}}{\sum_{t \in \mathcal{T}} \sum_{i \in \mathcal{I}} \sum_{j \in \mathcal{I}} \sum_{k \in \mathcal{K}} f_{ij,t}^k}, \quad (45)$$

is presented in Figure 3b. Additionally, we introduce the notion of cross-zone traffic to quantify the disparity between potential charging demand and actual charging demand. This metric, defined as

$$d_t = \frac{1}{\sum_{i \in \mathcal{I}} \Lambda_{i,t}} \left\| \Lambda_t - \sum_{k \in \mathcal{K}} \lambda_t^k \right\|_2, \quad (46)$$

provides a measure of the overall amount of relocation between zones due to drivers’ charging behaviors.

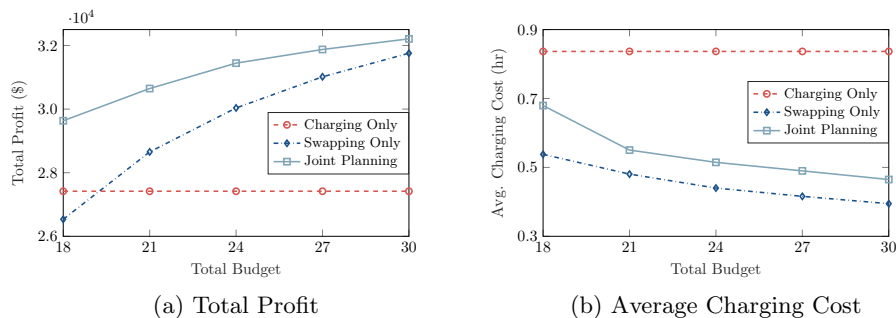


Figure 3: Performance of the infrastructure network under different deployment schemes.

On the one hand, battery swapping stations are costly and difficult to scale, while charging stations offer a more cost-effective solution for supporting a large EV fleet. Therefore, when the budget is limited,

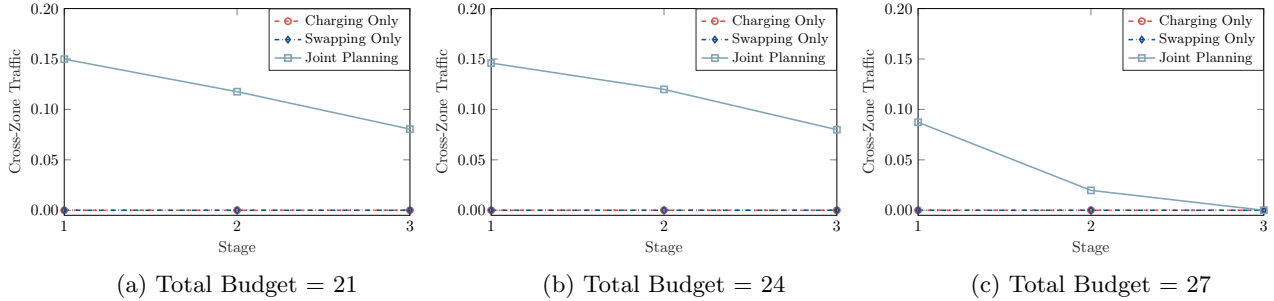


Figure 4: Distance between the potential charging demand and actual charging demand under different budget levels.

charging-only deployment yields a total profit that is 3.3% higher than swapping-only deployment. On the other hand, the long charging time poses an inherent bottleneck on plug-in charging, while battery swapping naturally overcomes this bottleneck with its much quicker turnaround. As a result, with a sufficient budget that can support an extensive swapping network, swapping-only deployment can lead to a substantial profit improvement of 15.8% and, at the same time, achieve a remarkable charging cost reduction of up to 52.8% compared to charging-only deployment.

In contrast, joint planning combines the advantages of both charging and battery swapping stations, thereby harnessing the synergistic value between the two facilities. Under the joint planning scheme, the platform can not only address the scaling challenge of battery swapping by building charging stations at the early stage but also overcome the bottleneck of plug-in charging and enhance fleet utilization by building battery swapping stations. Consequently, joint planning outperforms other deployment strategies in terms of profit maximization. However, the synergistic benefit of joint planning depends on the budget level as well as the scenario it is compared to. Specifically, under a tight budget, joint planning yields a total profit that is significantly higher than swapping-only deployment (i.e., by 11.7%). In this case, the major bottleneck is the budget as it is too limited to afford an extensive swapping network and thus cannot support a large EV fleet. Conversely, when the budget is generous, the bottleneck becomes the low fleet utilization arising from time-consuming plug-in charging. The total profit of joint planning is significantly higher than charging-only deployment under a large budget (i.e., by 17.5%). This is because by synergistically deploying charging and battery swapping stations, the platform can effectively reduce the charging cost and thus address this bottleneck. As shown in Figure 3b, compared to charging-only deployment, joint planning yields a charging cost reduction of up to 44.4% under a sufficient budget. As the budget increases, the charging cost of joint planning is even comparable to that of swapping only, which underscores the potential of joint planning to capitalize on the complementary strengths of charging and swapping facilities. We formalize the superiority of joint planning as follows.

Proposition 2. *The total profit of joint planning is always larger than or equal to that of charging-only or swapping-only deployment.*

Proof. Any charging-only deployment strategy can be interpreted as a joint planning strategy with the number of swapping stations being fixed at its initial value, i.e., $x_{i,t}^s = x_{i,0}^s, \forall t \in \mathcal{T}$, which is always a feasible solution to the original optimization problem (29). Therefore, the objective value under charging-only deployment will not be higher than that under joint planning. The same reasoning can be applied to swapping-only deployment as well. \square

The underlying reason is that charging or swapping-only deployment can be considered as a special case of joint planning. Its performance is equal to that of joint planning only when the optimal joint planning strategy falls on the boundary, where only one type of facility is built.

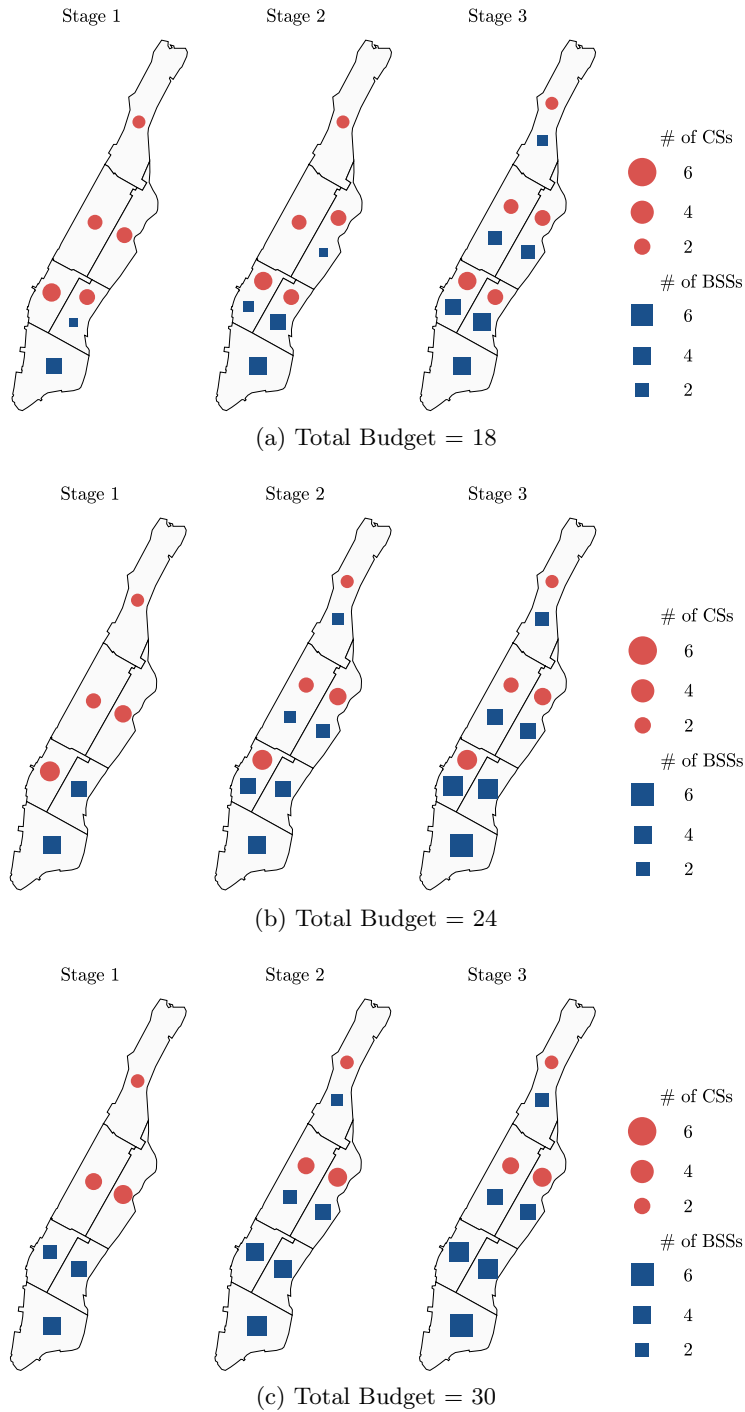


Figure 5: Infrastructure network expansion under different budget levels, with the red circles representing charging stations, the blue squares representing battery swapping stations, and their sizes representing the quantity of each type of facilities.

In addition, we also observe that a multimodal charging network can result in a significant increase in cross-zone traffic compared to a unimodal charging network. The primary reason for this gap is the substantial difference between charging time and swapping time. Plug-in charging typically takes around an hour, while battery swapping can be completed within a few minutes. Under a unimodal charging network, drivers do not have strong incentives to travel long distances for recharging. However, given a multimodal charging network, drivers can reduce their charging costs by relocating to a neighboring zone with a battery swapping station as long as the resulting increase in travel time is shorter than the time gap

between plug-in charging and battery swapping. Consequently, the volume of cross-zone traffic is higher under a joint planning strategy, particularly when the budget is insufficient to support an extensive battery swapping network, and the volume gradually decreases as the budget increases. These findings highlight the potential impacts of infrastructure planning on urban traffic congestion and management, which should be carefully considered and addressed when deploying a charging infrastructure network.

To investigate the robustness of our findings, we perform a comprehensive sensitivity analysis, in which multiple key parameters, such as the cost ratio between the two facilities, the discount factor and the penalty parameter, are varied within a reasonable range. Detailed results of the sensitivity analysis, as presented in [Appendix E](#), demonstrate the robustness of the superiority of joint planning. Across the various parameter settings tested, joint planning consistently outperforms alternative scenarios, which strengthens the argument for the effectiveness of joint planning.

5.4. Infrastructure Network Expansion

To further understand the benefits of joint planning, we present the expansion process of a mixed charging infrastructure network in [Figure 5](#). For better visualization, we re-partition Manhattan into 6 zones, with the upper three zones corresponding to areas with lower passenger demand and the lower three zones corresponding to areas with higher passenger demand.

It can be found that charging and battery swapping stations play different roles at different stages of long-term infrastructure planning. Due to the lower deployment cost, the platform prioritizes deploying charging stations at the early stage such that a dense charging network can be built to support a large EV fleet. As investment increases, the bottleneck of plug-in charging becomes increasingly apparent, necessitating an upgrade of the infrastructure network. The platform then deploys battery swapping stations to enhance fleet utilization. The expansion process highlights the complementary effect between the two facilities.

Another important observation is that the deployment priority of battery swapping stations is always assigned to areas with higher passenger demand. This is because charging demand is positively related to passenger demand in each zone. High-demand areas typically have high charging demand. In this light, the platform prefers to first build swapping facilities in high-demand areas where more EVs could use battery swapping for recharge, so the economical benefit associated with quicker turnaround and improved fleet utilization can be fully harnessed. Furthermore, by comparing [Figure 5a-5c](#), we can observe that the larger the budget level is, the fewer charging stations that will be built in the high-demand areas. These results also suggest that the platform should be far-sighted and avoid over-building charging stations in high-demand areas during the early stage, as this may lead to regret in the future when the budget is more abundant or when battery swapping is introduced. Overall, these discussions shed light on how demand and budget levels will affect the optimal deployment strategy and thus can advise infrastructure planning.

6. Extensions

6.1. Spatial Charging Equilibrium with Rejection

Since both the charging and battery swapping stations have finite capacities, newly arriving EVs may possibly get rejected if the queue is full. The proposed mathematical model is based on simplified settings where the queue capacity is assumed to be sufficiently large, resulting in a negligible blocking probability. However, in order to provide a more comprehensive model, we consider the scenario where rejection is taken into account. Let $v_{i,t}^k$ represent the blocking probability for mode k . All the rejected EVs should be relocated by choosing a charging mode and location again. The flow conservation conditions of these

rejected EVs can be represented as:

$$\begin{cases} \sum_{k \in \mathcal{K}} v_{i,t}^k \lambda_{i,t}^k = \sum_{j \in \mathcal{I}} \sum_{k \in \mathcal{K}} \hat{f}_{ij,t}^k, & (47a) \\ \hat{\lambda}_{i,t}^k = \sum_{j \in \mathcal{I}} \hat{f}_{ji,t}^k, & (47b) \end{cases}$$

where $\hat{f}_{ij,t}^k$ is the flow of the relocated EVs that are rejected due to limited queuing capacity, and $\hat{\lambda}_{ij,t}^k$ represents the arrival rates of relocated rejected flows to zone i . Therefore, the average arrival rate at each station is given by

$$\bar{\lambda}_{i,t}^k = \frac{1}{x_{i,t}^k} \left(\lambda_{i,t}^k + \hat{\lambda}_{i,t}^k \right), \quad (48)$$

which determines the waiting time $w_{i,t}^k$ and the blocking rate $v_{i,t}^k$ according to the queueing model. In this case, the charging cost is then defined as

$$c_{ij,t}^k = t_{ij} + (1 - v_{j,t}^k) \left(t_k + w_{j,t}^k \right) + v_{j,t}^k u_{j,t}, \quad (49)$$

where $u_{i,t}$ denotes the equilibrium charging cost for EVs from zone i . The spatial charging equilibrium is expressed by the following set of equations:

$$\begin{cases} f_{ij,t}^k, \hat{f}_{ij,t}^k \geq 0, & (50a) \\ c_{ij,t}^k - u_{i,t} \geq 0, & (50b) \\ f_{ij,t}^k (c_{ij,t}^k - u_{i,t}) = 0, & (50c) \\ \hat{f}_{ij,t}^k (c_{ij,t}^k - u_{i,t}) = 0. & (50d) \end{cases}$$

Note that the model implicitly assumes that each charging demand will not be blocked for more than once. However, in practice, an EV may experience multiple rejections before he/she successfully joins a queue (although the chance is rather small). One can easily account for the case of repeated rejections by introducing additional $\hat{f}_{ij,t}^k$ and $\hat{\lambda}_{i,t}^k$ following the same definitions. This model serves as a ‘‘first-order’’ approximation of the true case, which is sufficiently accurate given the observation that EVs will proactively choose a facility with a short waiting time and, consequently, a low blocking rate. The extended model is validated in a numerical study and the results are presented in [Appendix F](#). We find that (1) the first-order approximation adequately captures the charging rejection, with minimal discrepancies when compared to higher-order approximations; and (2) the simplified model aligns closely with the first-order approximation, indicating that overlooking charging rejection does not alter the qualitative outcomes of our analysis.

6.2. Spatial Charging Equilibrium with Differentiated Pricing

Considering the significantly shorter service time of battery swapping, EV drivers tend to over-utilize swapping stations, leading to extended waiting times such that the charging costs of the two modes are the same. It is reasonable to implement differentiated service fees for charging and battery swapping stations as a means to regulate demand. In light of this, we extend our proposed model to incorporate a differentiated pricing strategy. Let $s_{i,t}^k$ denote the service fee (measured in time) for mode k in zone i at stage t . Consequently, the charging cost is re-defined as

$$c_{i,t}^k = t_{ij} + t_k + w_{j,t}^k + s_{j,t}^k. \quad (51)$$

By directly adjusting the service fees for different modes across various locations, the platform can induce the desired charging behaviors. Our primary focus is to examine how the price differentiation between battery swapping and plug-in charging will impact market outcomes. To facilitate a fair comparison

between the simplified model and the extended model, we normalize the charging price to zero and use the price gap between battery swapping and plug-in charging, denoted as $s_{i,t} \geq 0$, as a decision. The positivity of $s_{i,t}$ arises from the observation that battery swapping is typically more expensive than plug-in charging. As such, the charging cost is modified as follows:

$$c_{i,t}^k = \begin{cases} t_{ij} + t_k + w_{j,t}^k, & \text{if } k = c, \\ t_{ij} + t_k + w_{j,t}^k + s_{j,t}, & \text{if } k = s. \end{cases} \quad (52a)$$

$$(52b)$$

If $s_{i,t} = 0$, the model degrades to the original one where EV drivers' decisions only depend on time costs. However, the platform may also set a positive price gap, i.e., $s_{i,t} > 0$, if it finds that the benefits of demand regulation outweigh the penalties associated with the increased equilibrium charging cost. We validate this extended model and compare its performance to the case without differentiated pricing in [Appendix F](#). Our results indicate that the implementation of differentiated pricing enhances the platform's flexibility in charging demand management, thereby leading to an improved profit. However, the improvement is insignificant, which is less than 1% for a large range of total budgets.

7. Conclusion

This study investigates the planning of a multimodal charging network, where charging stations and battery swapping stations are jointly deployed to support an electric ride-hailing fleet. A multi-stage charging network expansion model is formulated to capture how the platform makes infrastructure planning and operational decisions to maximize its profit. The model incorporates demand elasticity, spatial charging equilibrium, charging and swapping congestion, and other fundamental components in an electric ride-hailing market. A relaxed formulation is developed to establish a theoretical upper bound for the nonconcave joint deployment problem. Moreover, extensive numerical studies are conducted to validate the proposed model using real data from Manhattan.

Our findings indicate that joint planning charging and battery swapping stations can elicit synergistic value between the two facilities and yield a "one plus one more than two" benefit. Compared to deploying only one of them, joint planning not only addresses the scaling issue of battery swapping but also mitigates the inherent bottleneck associated with plug-in charging. At the early stage of infrastructure deployment, the platform prioritizes a dense network of charging stations that can support a large EV fleet. As the investment budget increases, the platform starts building battery swapping stations to improve fleet utilization and maximize profit. These results confirm the effectiveness of the proposed multimodal charging network. However, a multimodal charging network will lead to a larger volume of cross-zone traffic than a unimodal charging network, which highlights the potential impacts of infrastructure planning on traffic congestion and management. We also briefly discuss the deployment priority of battery swapping stations and show that this priority is always assigned to high-demand areas where more EVs can adopt battery swapping for recharging.

This study opens up several research directions that await further investigation. For instance, we focus on the steady-state performance in this work, whereas passenger demand varies over time in practice, and charging demand also changes accordingly. Therefore, a possible extension is to jointly consider the long-run planning decisions and real-time operational decisions. This can account for the temporal dynamics of passenger demand and charging demand, leading to more robust and efficient infrastructure planning solutions. Besides, drivers decide when to charge depending on the current state of charge, time-varying passenger demand, and the availability of charging facilities. It is therefore intriguing to explore how a mixed infrastructure network will reshape drivers' charging schedule when considering these real-time factors, and how to extend the model to explicitly characterize the interdependence between stationary charging demand and drivers' charging behaviors, which is a limitation of the current model. In addition,

this paper considers a ride-hailing platform collaborates with infrastructure providers to deploy charging infrastructure and demonstrates the economical benefits of such a partnership. While it remains unclear how these benefits would be divided between the two participants and how to ensure the stability of this partnership. These follow-up questions warrant further study. Moreover, future electric ride-hailing fleets could pose challenges and opportunities to urban power grids, especially considering the energy storage feature of battery swapping stations. So a dynamic charging and dispatching policy with integration of renewable energies is another interesting extension.

Acknowledgments

This research was supported by Hong Kong Research Grants Council under project 26200420, 16202922, and National Science Foundation of China under project 72201225.

References

- [1] Uber. Uber Q2 2022 Report, 2022. <https://investor.uber.com/news-events/news/press-release-details/2022/Uber-Announces-Results-for-Second-Quarter-2022/default.aspx>.
- [2] DiDi. DiDi’s Global Daily Trips Exceed 50 Million, 2020. <https://www.didiglobal.com/news/newsDetail?id=955&type=news>.
- [3] The Guardian. Electric cars account for under 5% of miles driven by Uber in Europe, 2021. <https://www.theguardian.com/technology/2021/nov/03/electric-cars-under-5-percent-miles-driven-uber-europe>.
- [4] Kelly L. Fleming and Mollie Cohen D’Agostino. Policy Pathways to TNC Electrification in California. Technical report, Institute of Transportation Studies, UC Davis, May 2020.
- [5] Alan Jenn. Emissions benefits of electric vehicles in Uber and Lyft ride-hailing services. *Nature Energy*, 5:520–525, July 2020.
- [6] Forbes. Uber, Lyft Have To Transition To Electric Vehicles In California, 2021. <https://www.forbes.com/sites/alanohnsman/2021/05/20/uber-lyft-have-to-transition-to-electric-vehicles-under-new-california-rule/?sh=7214e57a6f20>.
- [7] Uber. Together on the road to zero emissions. <https://www.uber.com/us/en/drive/services/electric>.
- [8] Lyft. Our commitment to achieve 100% electric vehicles across the lyft platform by 2030. <https://www.lyft.com/impact/electric>.
- [9] Angela Sanguinetti and Kenneth Kurani. Characteristics and Experiences of Ride-Hailing Drivers with Electric Vehicles. *World Electric Vehicle Journal*, 12(2):79, June 2021.
- [10] Zhichen Liu, Zhibin Chen, Yafeng Yin, and Zhengtian Xu. Regulatory policies to electrify ridesourcing systems. *Transportation Research Part C: Emerging Technologies*, 141:103743, August 2022.
- [11] Mohammad S. Roni, Zonggen Yi, and John G. Smart. Optimal charging management and infrastructure planning for free-floating shared electric vehicles. *Transportation Research Part D: Transport and Environment*, 76:155–175, November 2019.
- [12] Jason Plautz. Shenzhen, china touts nearly all-electric taxi fleet. <https://www.smartcitiesdive.com/news/electric-taxi-fleet-shenzhen-china/545347/>.

- [13] Jiri Opletal. Geely launched Cao Cao 60 EV with swappable batteries and a 415 km range for \$17,500. <https://carnewschina.com/2023/03/30/geely-launched-cao-cao-60-ev-with-swappable-batteries-and-a-415-km-range-for-17500/>.
- [14] South China Morning Post. China's Didi Chuxing launches first electric vehicle tailored for ride-sharing services. <https://www.scmp.com/tech/start-ups/article/3110132/chinas-didi-chuxing-launches-first-electric-vehicle-tailored-ride>.
- [15] The Wall Street Journal. Uber Working With Auto Makers to Design EVs Customized for Ride-Sharing, Delivery. <https://www.wsj.com/articles/uber-working-with-auto-makers-to-design-vehicles-customized-for-ride-sharing-delivery-11674132796>.
- [16] CNBC. Uber to offer autonomous ride-hailing and delivery services using waymo's robotaxis. <https://www.cnbc.com/2023/05/23/uber-and-waymo-team-up-on-robotaxi-ride-hailing-and-delivery-services.html>.
- [17] Reuters. China's Didi Global to roll out self-developed robotaxis by 2025. <https://www.reuters.com/business/autos-transportation/chinas-didi-global-roll-out-self-developed-robotaxis-by-2025-2023-04-13/>.
- [18] ChinaDaily. Oil giant teams up with aulton to build battery swap stations. <https://global.chinadaily.com.cn/a/202111/15/WS6191a703a310cdd39bc7548d.html>.
- [19] Ample. Accelerating the move to EVs. <https://ample.com/fleets/#learn-about-ample>.
- [20] Jintao Ke, Xuekai Cen, Hai Yang, Xiqun Chen, and Jieping Ye. Modelling drivers' working and recharging schedules in a ride-sourcing market with electric vehicles and gasoline vehicles. *Transportation Research Part E: Logistics and Transportation Review*, 125:160–180, May 2019.
- [21] Xiaoran Qin, Kaixian Yu, Hanqian Li, Feng Dai, Haijiang Liu, Hai Yang, Jieping Ye, and Hongtu Zhu. Development of a one-day driving cycle for electric ride-hailing vehicles. *Transportation Research Part D: Transport and Environment*, 89:102597, December 2020.
- [22] Md Rakibul Alam, Chuang Hou, Spencer Aeschliman, Yan Zhou, and Zhaomiao Guo. Optimization-based trip chain emulation for electrified ride-sourcing charging demand analyses. *Transportation Letters*, 0(0):1–17, May 2022.
- [23] Jie Shi, Yuanqi Gao, Wei Wang, Nanpeng Yu, and Petros A. Ioannou. Operating Electric Vehicle Fleet for Ride-Hailing Services With Reinforcement Learning. *IEEE Transactions on Intelligent Transportation Systems*, 21(11):4822–4834, November 2020.
- [24] Nicholas D. Kullman, Martin Cousineau, Justin C. Goodson, and Jorge E. Mendoza. Dynamic Ride-Hailing with Electric Vehicles. *Transportation Science*, 56(3):775–794, May 2022.
- [25] Ji Hyun Hong and Xiaoxi Liu. The optimal pricing for green ride services in the ride-sharing economy. *Transportation Research Part D: Transport and Environment*, 104:103205, March 2022.
- [26] Yanyan Ding, Sen Li, and Sisi Jian. Optimal pricing and fleet management for shared electric vehicle in coupled power and transport networks. *Transportation Research Part C: Emerging Technologies*, 141:103727, August 2022.
- [27] Zeen Cai, Dong Mo, Maosi Geng, Wei Tang, and Xiqun Michael Chen. Integrating ride-sourcing with electric vehicle charging under mixed fleets and differentiated services. *Transportation Research Part E: Logistics and Transportation Review*, 169:102965, January 2023.

- [28] T. Donna Chen, Kara M. Kockelman, and Josiah P. Hanna. Operations of a shared, autonomous, electric vehicle fleet: Implications of vehicle & charging infrastructure decisions. *Transportation Research Part A: Policy and Practice*, 94:243–254, December 2016.
- [29] Berkay Turan, Ramtin Pedarsani, and Mahnoosh Alizadeh. Dynamic pricing and fleet management for electric autonomous mobility on demand systems. *Transportation Research Part C: Emerging Technologies*, 121:102829, December 2020.
- [30] Zonggen Yi and John Smart. A framework for integrated dispatching and charging management of an autonomous electric vehicle ride-hailing fleet. *Transportation Research Part D: Transport and Environment*, 95:102822, June 2021.
- [31] Lina Al-Kanj, Juliana Nascimento, and Warren B. Powell. Approximate dynamic programming for planning a ride-hailing system using autonomous fleets of electric vehicles. *European Journal of Operational Research*, 284(3):1088–1106, August 2020.
- [32] Peter Slowik, Sandra Wappelhorst, and Nicholas Lutsey. How can taxes and fees on ride-hailing fleets steer them to electrify? Technical report, International Council on Clean Transportation, 2019.
- [33] Dong Mo, Jingru Yu, and Xiquan Michael Chen. Modeling and managing heterogeneous ride-sourcing platforms with government subsidies on electric vehicles. *Transportation Research Part B: Methodological*, 139:447–472, September 2020.
- [34] Dale Hall, Mike Nicholas, and Marie Rajon Bernard. Guide to electrifying ride-hailing vehicles for cities. *Working Paper*, 2021.
- [35] Leah Lazer, Sadanand Wachche, Ryan Sclar, and Sarah Cassius. Electrifying Ride-Hailing in the United States, Europe, and Canada: How to Enable Ride-Hailing Drivers to Switch to Electric Vehicles. Technical report, World Resources Institute, 2021.
- [36] Zuo-Jun Max Shen, Bo Feng, Chao Mao, and Lun Ran. Optimization models for electric vehicle service operations: A literature review. *Transportation Research Part B: Methodological*, 128:462–477, October 2019.
- [37] Georg Brandstätter, Michael Kahr, and Markus Leitner. Determining optimal locations for charging stations of electric car-sharing systems under stochastic demand. *Transportation Research Part B: Methodological*, 104:17–35, October 2017.
- [38] Tai-Yu Ma and Simin Xie. Optimal fast charging station locations for electric ridesharing with vehicle-charging station assignment. *Transportation Research Part D: Transport and Environment*, 90:102682, January 2021.
- [39] Md Rakibul Alam and Zhaomiao Guo. Charging infrastructure planning for ride-sourcing electric vehicles considering drivers’ value of time. *Transportation Letters*, 0:1–11, May 2022.
- [40] Gordon S. Bauer, Amol Phadke, Jeffery B. Greenblatt, and Deepak Rajagopal. Electrifying urban ridesourcing fleets at no added cost through efficient use of charging infrastructure. *Transportation Research Part C: Emerging Technologies*, 105:385–404, August 2019.
- [41] Alan Jenn. Charging Forward: Deploying Electric Vehicle Infrastructure for Uber and Lyft in California. Technical report, UC Davis: Institute of Transportation Studies, 2021.
- [42] Ho-Yin Mak, Ying Rong, and Zuo-Jun Max Shen. Infrastructure Planning for Electric Vehicles with Battery Swapping. *Management Science*, 59(7):1557–1575, July 2013. Publisher: INFORMS.

- [43] Yang Wang, Wenjian Ding, Liusheng Huang, Zheng Wei, Hengchang Liu, and John A. Stankovic. Toward Urban Electric Taxi Systems in Smart Cities: The Battery Swapping Challenge. *IEEE Transactions on Vehicular Technology*, 67(3):1946–1960, March 2018.
- [44] William Infante, Jin Ma, Xiaoqing Han, and Ariel Liebman. Optimal Recourse Strategy for Battery Swapping Stations Considering Electric Vehicle Uncertainty. *IEEE Transactions on Intelligent Transportation Systems*, 21(4):1369–1379, April 2020.
- [45] Xiong Yang, Chunfu Shao, Chengxiang Zhuge, Mingdong Sun, Pinxi Wang, and Shiqi Wang. Deploying battery swap stations for shared electric vehicles using trajectory data. *Transportation Research Part D: Transport and Environment*, 97:102943, August 2021.
- [46] Joon Moon, Young Joo Kim, Taesu Cheong, and Sang Hwa Song. Locating Battery Swapping Stations for a Smart e-Bus System. *Sustainability*, 12(3):1142, January 2020.
- [47] Jie Zhang, Lihui Bai, and Tongdan Jin. Joint planning for battery swap and supercharging networks with priority service queues. *International Journal of Production Economics*, 233:108009, March 2021.
- [48] Xu Zhang, Linyu Peng, Yue Cao, Shuohan Liu, Huan Zhou, and Keli Huang. Towards holistic charging management for urban electric taxi via a hybrid deployment of battery charging and swap stations. *Renewable Energy*, 155:703–716, August 2020.
- [49] BP. BP and DiDi join forces to build electric vehicle charging network in China. <https://www.bp.com/en/global/corporate/news-and-insights/press-releases/bp-and-didi-join-forces-to-build-electric-vehicle-charging-network-in-china.html>.
- [50] Businesswire. Uber and Wallbox to expand partnership to all of the U.S. <https://www.businesswire.com/news/home/20220201005729/en/Uber-and-Wallbox-to-Expand-Partnership-to-All-of-The-U.S>.
- [51] Ample. Announcing a New Ride Sharing EV Experience with Sally. <https://ample.com/2021/06/10/announcing-a-new-ride-sharing-ev-experience-with-sally/>.
- [52] Zeyi Yang. China plans charging infrastructure for 20 million EVs. <https://www.protocol.com/bulletins/china-infrastructure-plan-ev>.
- [53] EVbox. Ev charging infrastructure incentives in Europe 2022. <https://blog.evbox.com/ev-charging-infrastructure-incentives-eu#:~:text=A%2045%20percent%20personal%20income,charging%20point%20and%20per%20taxpayer>.
- [54] Yaqian Zhou, Hai Yang, Jintao Ke, Hai Wang, and Xinwei Li. Competition and third-party platform-integration in ride-sourcing markets. *Transportation Research Part B: Methodological*, 159:76–103, May 2022.
- [55] Qi (George) Chen, Yanzhe (Murray) Lei, and Stefanus Jasin. Real-Time Spatial–Intertemporal Pricing and Relocation in a Ride-Hailing Network: Near-Optimal Policies and the Value of Dynamic Pricing. *Operations Research*, April 2023.
- [56] Richard Arnott. Taxi travel should be subsidized. *Journal of Urban Economics*, 40(3):316–333, 1996.
- [57] Sen Li, Hamidreza Tavafoghi, Kameshwar Poolla, and Pravin Varaiya. Regulating TNCs: Should Uber and Lyft set their own rules? *Transportation Research Part B: Methodological*, 129:193–225, November 2019.
- [58] Juan Camilo Castillo, Dan Knoepfle, and Glen Weyl. Surge pricing solves the wild goose chase. In *Proceedings of the 2017 ACM Conference on Economics and Computation*, page 241–242, 2017.

- [59] Jintao Ke, Hai Yang, Xinwei Li, Hai Wang, and Jieping Ye. Pricing and equilibrium in on-demand ride-pooling markets. *Transportation Research Part B: Methodological*, 139:411–431, 2020.
- [60] Xinwu Qian, Jiawei Xue, Stanislav Sobolevsky, Chao Yang, and Satish Ukkusuri. Stationary Spatial Charging Demand Distribution for Commercial Electric Vehicles in Urban Area. In *2019 IEEE Intelligent Transportation Systems Conference (ITSC)*, pages 220–225, October 2019.
- [61] Gilbert Strang. *Introduction to Linear Algebra*, volume 3. Wellesley-Cambridge Press, 1993.
- [62] Frederick S. Hillier and Gerald J. Lieberman. *Introduction to Operations Research*. McGraw-Hill Higher Education, July 2004.
- [63] Xiaoqi Tan, Bo Sun, and Danny H. K. Tsang. Queueing network models for electric vehicle charging station with battery swapping. In *2014 IEEE International Conference on Smart Grid Communications (SmartGridComm)*, pages 1–6, November 2014.
- [64] Yuping Lin, Kai Zhang, Zuo-Jun Max Shen, Bin Ye, and Lixin Miao. Multistage large-scale charging station planning for electric buses considering transportation network and power grid. *Transportation Research Part C: Emerging Technologies*, 107:423–443, October 2019.
- [65] Stefan Scholtes. Convergence Properties of a Regularization Scheme for Mathematical Programs with Complementarity Constraints. *SIAM Journal on Optimization*, 11(4):918–936, January 2001.
- [66] Jeff X. Ban, Henry X. Liu, Michael C. Ferris, and Bin Ran. A general MPCC model and its solution algorithm for continuous network design problem. *Mathematical and Computer Modelling*, 43(5):493–505, March 2006.
- [67] Rui Chen, Xinwu Qian, Lixin Miao, and Satish V. Ukkusuri. Optimal charging facility location and capacity for electric vehicles considering route choice and charging time equilibrium. *Computers & Operations Research*, 113:104776, January 2020.
- [68] Dimitri Bertsekas. *Nonlinear Programming*. Athena Scientific, 3rd edition, 2016.
- [69] TLC Trip Record Data - TLC. <https://www1.nyc.gov/site/tlc/about/tlc-trip-record-data.page>.
- [70] Michael Nicholas. Estimating electric vehicle charging infrastructure costs across major U.S. metropolitan areas. <https://theicct.org/publication/estimating-electric-vehicle-charging-infrastructure-costs-across-major-u-s-metropolitan-areas/>.
- [71] SCMP. Chinese smart-battery swap stations can change ev batteries automatically. <https://www.scmp.com/video/scmp-originals/3168635/chinese-smart-battery-swap-stations-can-change-ev-batteries>.
- [72] Andrei Nedelea. Take A Closer Look At A Nio EV Battery Swapping Station In China. <https://insideevs.com/news/570403/nio-battery-swap-station-china/>.
- [73] CNBC. How much money NYC Uber, Lyft and Juno drivers can earn in a day. <https://www.cnbc.com/2019/02/04/how-much-money-nyc-uber-lyft-and-juno-drivers-can-earn-in-a-day.html>.
- [74] Tian Lei, Shuocheng Guo, Xinwu Qian, and Lei Gong. Understanding charging dynamics of fully-electrified taxi services using large-scale trajectory data. *Transportation Research Part C: Emerging Technologies*, 143:103822, 2022.

Appendix A. Parameter Settings

To ensure a realistic representation of charging infrastructure, we calibrate the relevant parameters based on industry practices. For instance, it is suggested that around 70% of charging stations in US metropolitan areas have less than six chargers [70]. Therefore, we assume each charging station in our model has five chargers. Furthermore, taking NIO’s battery swapping station as a reference, we set the number of swapping slots to 1 [71]. In particular, charging and swapping stations are assumed to have the same configuration for a fair comparison. We thus consider each battery swapping station has five chargers and five batteries in circulation. The average charging time is 40 minutes, while each swapping session lasts 5 minutes. To minimize the impact of blocking, we assume both facilities have a queue capacity of 50. The upper bounds for the arrival rate at both facilities, i.e., ρ_k , are selected to result in an average waiting time of 1 hour (See Appendix C for more details). In terms of deployment costs, we decide the value based on infrastructure configuration. An estimation from 2019 [70] indicates that the cost of deploying each 50kW DC fast charger in U.S. metropolitan areas is approximately \$40,000, depending on the location, technology used, and other factors. Hence, the total cost of a charging station with five chargers amounts to \$200,000 (note that the cost of the charging station depends on its configuration, i.e., number of chargers). We apportion this cost to an hourly basis over a one-year period and assume $\gamma_c = \$20$. While building each battery swapping station costs around \$500,000 according to NIO [72]. Taking into account NIO’s technological advantages and economies of scale, as well as higher land acquisition costs in Manhattan, we assume the cost of building a battery swapping station is five times that of a charging station with the same configuration, i.e., five chargers and five batteries, so that the cost of battery swapping station also depends on its configuration (i.e., number of chargers inside). The operational cost of EVs is set to be \$25/hr based on the hourly earnings of Uber drivers in NYC [73]. We consider each stage spans one year and set the discount factor as 0.9. Additionally, instead of tuning $(\varepsilon, \omega, \Omega)$ separately in (11), we fix $(1 - \varepsilon)\Omega/\omega = 8$, meaning that EVs can sustain for eight hours between two top-ups. This is close to the charging pattern of a large-scale electric taxi fleet [74].

Table A.2: Summary of model parameters

Parameter	Description	Value
γ_e	operational cost of each EV	\$25/hr
γ_c	deployment cost of each charging station	\$20/hr
γ_s	deployment cost of each battery swapping station	\$100/hr
γ_p	penalty parameter for the total charging cost	\$20/hr
γ	discount factor in the objective function	0.9
ϕ	parameters in the pickup time model	1/3
α	sensitivity parameter in the demand model	0.12
β	passengers’ value of time	\$90/hr
t_c	average charging time	40 min
t_s	constant swapping time	5 min
C	number of chargers in each station	5
S	number of swapping slots in each station	1
B	number of batteries at each swapping station	5
K	queue capacity of each station	50
ρ_c	upper bound for the arrival rate at charging stations	6.767
ρ_s	upper bound for the arrival rate at swapping stations	5.499
T	number of stages in the planning horizon	3
H	number of stages in the operation horizon	6
$(1 - \varepsilon)\Omega/\omega$	charging frequency of each EV	8

Appendix B. Stationary Distribution of Swapping Queue

As indicated in [63], the steady-state distribution of the swapping queue can be conveniently computed in matrix form without solving a linear equation system. Specifically, we can obtain $G(i, j)$ by simply solving $G\Pi = G$, where $G = [G(0, 0), \dots, G(0, B), \dots, G(K, 0), \dots, G(K, B)]$ is a row vector and Π is the transition matrix of the embedded Markov chain. To construct the matrix Π , we define the following $(B + 1) \times (B + 1)$ matrix Δ :

$$\Delta = \left[\begin{array}{ccc|ccc} f(0,0) & \cdots & 0 & 0 & \cdots & 0 \\ \vdots & \ddots & \vdots & \vdots & \vdots & \vdots \\ f(C,0) & \cdots & f(C,C) & 0 & \cdots & 0 \\ f(C,0) & \cdots & f(C,C) & 0 & \cdots & 0 \\ \vdots & \ddots & \vdots & \vdots & \vdots & \vdots \\ f(C,0) & \cdots & f(C,C) & 0 & \cdots & 0 \end{array} \right], \quad (\text{B.1})$$

where $f(i, j)$ is given by (20). As such, any infeasible transition can be easily excluded by 0 entries in the matrix. Then the transition matrix Π can be constructed as follows:

Algorithm 1: Construction of matrix Π

```

1 for  $i \leftarrow 1$  to  $(K + 1) \times (B + 1)$  do
2   for  $j \leftarrow 1$  to  $(K + 1) \times (B + 1)$  do
3      $a = \lfloor (i - 1) / (B + 1) \rfloor$ 
4      $b = (i - 1) \bmod (B + 1)$ 
5      $m = \lfloor (j - 1) / (B + 1) \rfloor$ 
6      $n = (j - 1) \bmod (B + 1)$ 
7      $\delta = \begin{cases} g(m - 1 - a + \min\{a, b, S\}), & \text{if } m < K - 1 \\ 1 - \sum_{l=0}^{K-1} g(l - a + \min\{a, b, S\}), & \text{if } m = K - 1 \end{cases}$ 
8      $\Pi(i, j) = \delta \cdot \Delta(B - b + 1, n - b + \min\{a, b, S\})$ 
9   end
10 end
```

Appendix C. Performance of Queueing Models

Figure C.6 and Figure C.7 show the waiting time and blocking rate of both charging and swapping queues under different EV arrival rates. It can be found that when the waiting time is in a tolerable range, e.g., less than 1 hour, the blocking rate is negligible. To ensure acceptable waiting times, we impose constraint (24), which sets an upper bound on the EV arrival rate. This constraint limits the arrival rate such that the resulting waiting time is kept below 1 hour. As summarized in Table C.3, with a sufficiently large queue capacity, the blocking rate is marginal, e.g., less than 0.1%, for any arrival rate below its upper bound. These results illustrate that we can effectively prevent the case of a full queue by properly limiting the maximum EV arrival rate and meanwhile choosing a suitable queue capacity.

Table C.3: EV arrival rate and the blocking rate when the waiting time is 1 hour.

K	ρ_c	Blocking Rate	ρ_s	Blocking Rate
30	6.965	1.055%	5.546	0.278%
40	6.814	0.255%	5.510	0.063%
50	6.767	0.074%	5.499	0.016%

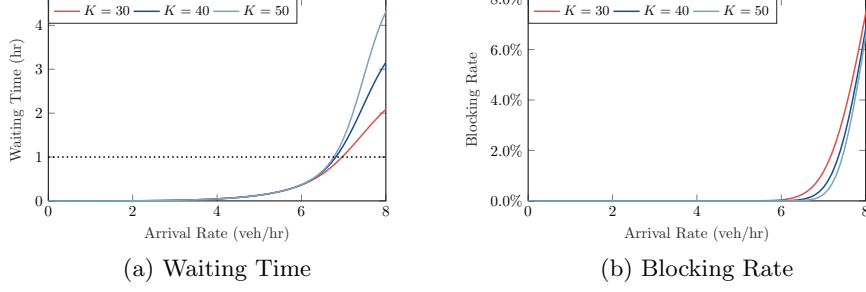


Figure C.6: Queuing performance of a charging station.

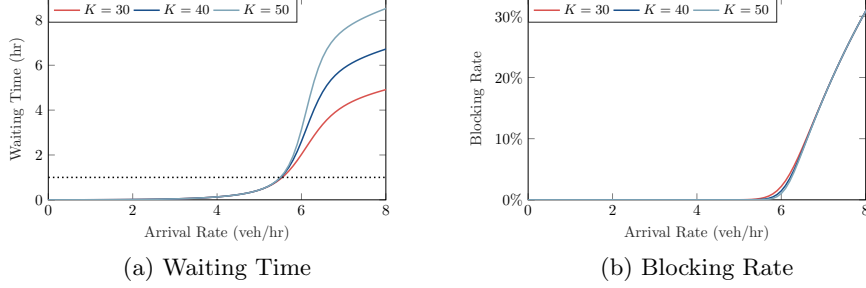


Figure C.7: Queuing performance of a battery swapping station.

Appendix D. Derivation of Benchmark Upper Bounds

Aside from the proposed method, another upper bound is established as a benchmark via Lagrangian relaxation. To obtain a decomposable structure from the original problem, we first insert (9) into (8):

$$\sum_{i \in \mathcal{I}} \Lambda_{i,t} P_{ij,t} = \Lambda_{j,t}, \quad (\text{D.1})$$

which is clearly separable over i because $P_{ij,t}$ only depends on $N_{i,t}^v, q_{ij,t}, r_{ij,t}, \forall j \in \mathcal{I}$. Note that the energy balance condition also has a separable structure. For ease of notation, we combine (D.1) and (11) as $H_{v,t} = \sum_{i \in \mathcal{I}} H_{vi,t} = 0$, where $H_{vi,t}$ is a function of $\{N_{i,t}^v, q_{ij,t}, r_{ij,t}, f_{ij,t}^k\}_{\forall j \in \mathcal{I}, k \in \mathcal{K}}$. Moreover, we linearize the complementarity constraint (14c) by introducing a binary variable $z_{ij,t}^k$:

$$\begin{cases} z_{ij,t}^k \in \{0, 1\}, & (\text{D.2a}) \\ f_{ij,t}^k \leq M(1 - z_{ij,t}^k), & (\text{D.2b}) \\ c_{ij,t}^k - u_{i,t} \leq Mz_{ij,t}^k, & (\text{D.2c}) \end{cases}$$

where M is a sufficiently large constant. This is equivalent to the original complementarity constraint in the sense that when $f_{ij,t}^k > 0$, $z_{ij,t}^k$ must be 0, and thus $c_{ij,t}^k = u_{i,t}$. The equilibrium conditions (14) then becomes separable since $c_{ij,t}^k$ only depends on $\lambda_{j,t}^k$. To ensure the satisfaction of constraint qualification, we further relax (D.2c) as in (30):

$$c_{ij,t}^k - u_{i,t} \leq Mz_{ij,t}^k + \epsilon. \quad (\text{D.3})$$

As such, the original optimization problem becomes a mixed-integer nonlinear program that is subject to the following coupled constraints:

$$\sum_{i \in \mathcal{I}} \sum_{k \in \mathcal{K}} \gamma_k x_{i,t}^k \leq b_t, \quad \forall t \in \mathcal{T}, \quad (\text{D.4a})$$

$$x_{i,t}^k - x_{i,t-1}^k \geq 0, \quad \forall t \in \mathcal{T}, i \in \mathcal{I}, k \in \mathcal{K}, \quad (\text{D.4b})$$

$$\lambda_{i,t}^k = \sum_{j \in \mathcal{I}} f_{ji,t}^k, \quad \forall t \in \mathcal{T}, i \in \mathcal{I}, k \in \mathcal{K}, \quad (\text{D.4c})$$

$$H_{v,t} = \sum_{i \in \mathcal{I}} H_{vi,t} = 0, \quad \forall t \in \mathcal{T}, v \in \mathcal{V}, \quad (\text{D.4d})$$

$$c_{ij,t}^k - u_{i,t} \geq 0, \quad \forall t \in \mathcal{T}, i \in \mathcal{I}, j \in \mathcal{I}, k \in \mathcal{K}, \quad (\text{D.4e})$$

$$c_{ij,t}^k - u_{i,t} \leq M z_{ij,t}^k + \epsilon, \quad \forall t \in \mathcal{T}, i \in \mathcal{I}, j \in \mathcal{I}, k \in \mathcal{K}, \quad (\text{D.4f})$$

$$\sum_{j \in \mathcal{I}} (q_{ij,t} + r_{ij,t}) = \sum_{j \in \mathcal{I}} (q_{ji,t} + r_{ji,t}), \quad \forall t \in \mathcal{T}, i \in \mathcal{I}. \quad (\text{D.4g})$$

Let $\Phi = (\eta, \delta, \nu, \theta, \psi, \phi, \mu)$ denote the Lagrange multipliers associated with these constraints. We then have the separable partial Lagrangian as follows:

$$\begin{aligned} \mathcal{L} = & \sum_{t \in \mathcal{T}} (\sigma_t^r \Pi_t^r - \sigma_t^c \Pi_t^c) - \sum_{t \in \mathcal{T}} \sum_{i \in \mathcal{I}} \sum_{k \in \mathcal{K}} \eta_t \gamma_k x_{i,t}^k + \sum_{t \in \mathcal{T}} \sum_{i \in \mathcal{I}} \sum_{k \in \mathcal{K}} \nu_{i,t}^k \left(\lambda_{i,t}^k - \sum_{j \in \mathcal{I}} f_{ji,t}^k \right) \\ & + \sum_{t \in \mathcal{T}} \sum_{i \in \mathcal{I}} \sum_{j \in \mathcal{I}} \sum_{k \in \mathcal{K}} \psi_{ij,t}^k \left(c_{ij,t}^k - u_{i,t} \right) - \sum_{t \in \mathcal{T}} \sum_{i \in \mathcal{I}} \sum_{j \in \mathcal{I}} \sum_{k \in \mathcal{K}} \phi_{ij,t}^k \left(c_{ij,t}^k - u_{i,t} - M z_{ij,t}^k \right) \\ & + \sum_{t \in \mathcal{T}} \sum_{i \in \mathcal{I}} \sum_{k \in \mathcal{K}} \delta_{i,t}^k (x_{i,t}^k - x_{i,t-1}^k) + \sum_{t \in \mathcal{T}} \sum_{i \in \mathcal{I}} \sum_{v \in \mathcal{V}} \theta_{v,t} H_{vi,t} + \sum_{t \in \mathcal{T}} \sum_{i \in \mathcal{I}} \sum_{j \in \mathcal{I}} (\mu_{i,t} - \mu_{j,t}) (q_{ij,t} + r_{ij,t}) \end{aligned} \quad (\text{D.5})$$

The decomposable structure of this Lagrangian allows us to define multiple subproblems, each of which is a function of $(x_{i,t}^k, u_{i,t}, \Lambda_{i,t}, \lambda_{i,t}^k, N_{i,t}^v, q_{ij,t}, r_{ij,t}, f_{ij,t}^k, z_{ij,t}^k), \forall j \in \mathcal{I}, k \in \mathcal{K}$. Furthermore, each subproblem can be divided into two classes of smaller-scale problems that can be independently solved.

The first class is a bi-variate optimization of $x_{i,t}^k$ and $\lambda_{i,t}^k$:

$$\begin{aligned} & \underset{x_{i,t}^k, \lambda_{i,t}^k}{\text{maximize}} \quad \left[\gamma_k (\sigma_{t+1}^c - \sigma_t^c - \eta_t) + (\delta_{i,t}^k - \delta_{i,t+1}^k) \right] x_{i,t}^k + \nu_{i,t}^k \lambda_{i,t}^k \\ & \quad - \sigma_t^r \gamma_e \lambda_{i,t}^k (w_{i,t}^k + t_k) + \sum_{j \in \mathcal{I}} (\psi_{ji,t}^k - \phi_{ji,t}^k) w_{i,t}^k \\ & \text{subject to} \quad x_{i,0}^k \leq x_{i,t}^k \leq \bar{x}_i^k, \\ & \quad \quad \quad 0 \leq \lambda_{i,t}^k \leq \rho_k x_{i,t}^k. \end{aligned} \quad (\text{D.6})$$

Such a two-dimensional maximization problem can be efficiently solved even in the absence of concavity.

The second class is a mixed-integer nonlinear program over $(u_{i,t}, \Lambda_{i,t}, N_{i,t}^v, q_{ij,t}, r_{ij,t}, f_{ij,t}^k, z_{ij,t}^k), \forall j \in \mathcal{I}, k \in \mathcal{K}$:

$$\begin{aligned}
& \underset{\substack{u_{i,t}, \Lambda_{i,t}, N_{i,t}^v, q_{ij,t}, \\ r_{ij,t}, f_{ij,t}^k, z_{ij,t}^k}}{\text{maximize}} & \sigma_t^r \sum_{j \in \mathcal{I}} p_{ij,t} q_{ij,t} - \sigma_t^r \gamma_e \sum_{j \in \mathcal{I}} q_{ij,t} w_{i,t}^p - \sigma_t^r \gamma_e \sum_{j \in \mathcal{I}} \left(q_{ij,t} + r_{ij,t} + \sum_{k \in \mathcal{K}} f_{ij,t}^k \right) t_{ij} \\
& - \sigma_t^r \gamma_e N_{i,t}^v - \sigma_t^r \gamma_p \Lambda_{i,t} u_{i,t} + \sum_{v \in \mathcal{V}} \theta_{v,t} H_{vi,t} + \sum_{j \in \mathcal{I}} (\mu_{i,t} - \mu_{j,t}) (q_{ij,t} + r_{ij,t}) \\
& - \sum_{j \in \mathcal{I}} \sum_{k \in \mathcal{K}} \nu_{j,t}^k f_{ij,t}^k + \sum_{j \in \mathcal{I}} \sum_{k \in \mathcal{K}} (\phi_{ij,t}^k - \psi_{ij,t}^k) u_{i,t} + M \sum_{j \in \mathcal{I}} \sum_{k \in \mathcal{K}} \phi_{ij,t}^k z_{ij,t}^k \\
& \text{subject to} & N_{i,t}^v > \hat{N}^v, \\
& & q_{ij,t} > 0, \quad \forall j \in \mathcal{I}, \\
& & \Lambda_{i,t} = \sum_{k \in \mathcal{K}} \sum_{j \in \mathcal{I}} f_{ij,t}^k, \\
& & z_{ij,t}^k \in \{0, 1\}, \quad \forall j \in \mathcal{I}, k \in \mathcal{K}, \\
& & f_{ij,t}^k \leq M(1 - z_{ij,t}^k), \quad \forall j \in \mathcal{I}, k \in \mathcal{K}.
\end{aligned} \tag{D.7}$$

We notice that complexities of the objective function mainly arise from $H_{vi,t}$. However, if $\Lambda_{i,t}$, $N_{i,t}^v$, and $\sum_{j \in \mathcal{I}} q_{ij,t} w_{i,t}^p + \sum_{j \in \mathcal{I}} (q_{ij,t} + r_{ij,t}) t_{ij}$ are fixed, $H_{vi,t}$ is simplified to a linear function of $q_{ij,t}$, $r_{ij,t}$ and $f_{ij,t}^k$. This problem consequently becomes a concave program over $q_{ij,t}$ and a mixed-integer linear program over other decisions. We can therefore perform a brute-force search over a three-dimensional space and then efficiently solve the two residual programs using off-the-shelf solvers.

Following the principle of Lagrangian relaxation, we obtain a valid upper bound for the original problem by optimally solving (D.6) and (D.7) for all $i \in \mathcal{I}$ and $t \in \mathcal{T}$. This bound is utilized as a benchmark to evaluate the performance of our proposed bound.

Appendix E. Results of Sensitivity Analysis

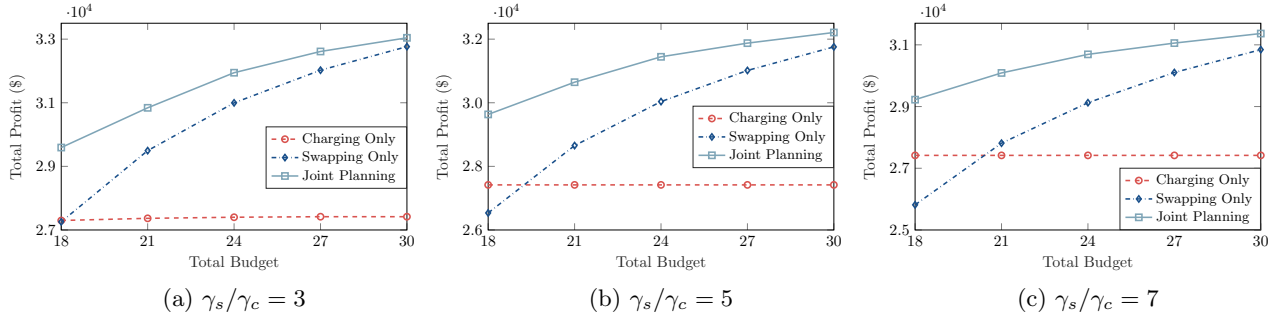


Figure E.8: Performance under different cost ratios between battery swapping stations and charging stations.

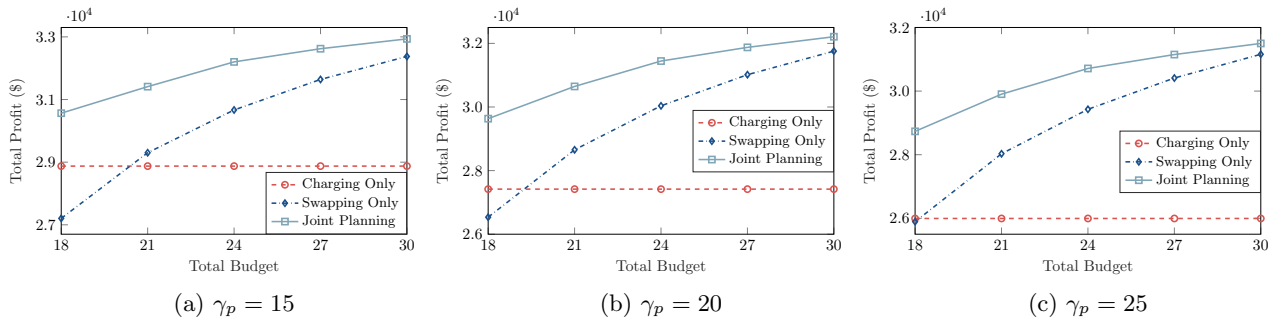


Figure E.9: Performance under different values of the penalty parameter γ_p .

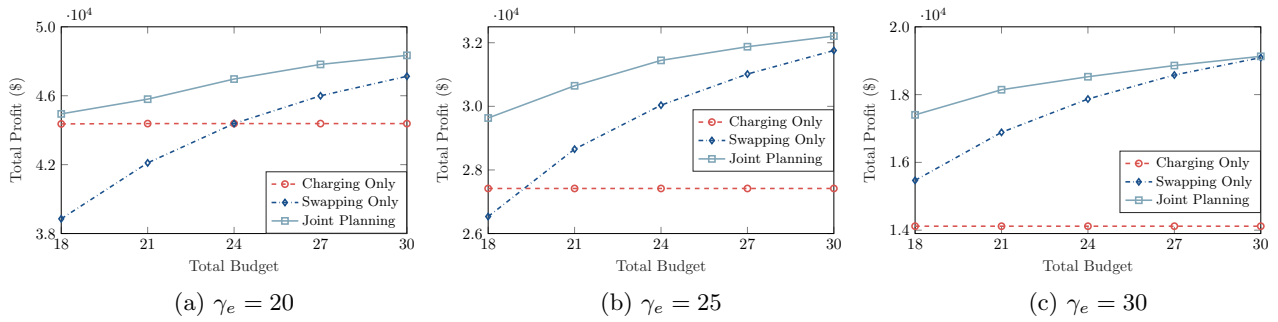


Figure E.10: Performance under different values of the vehicle cost γ_e .

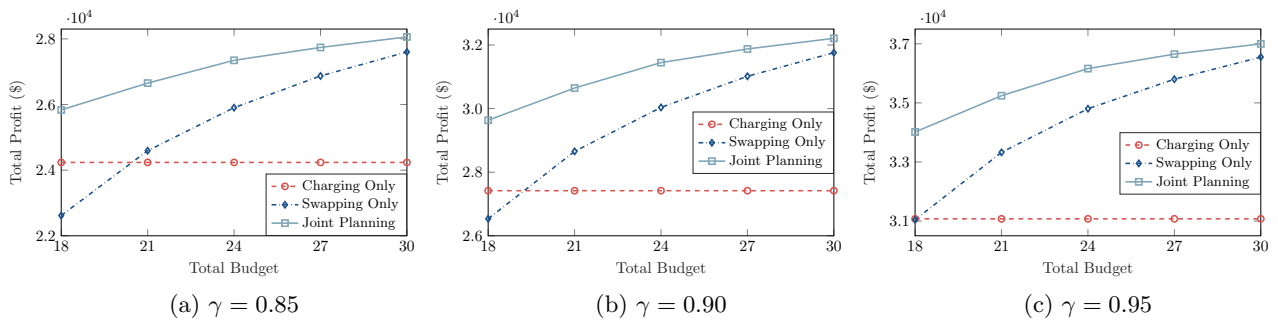


Figure E.11: Performance under different values of the discount factor γ .

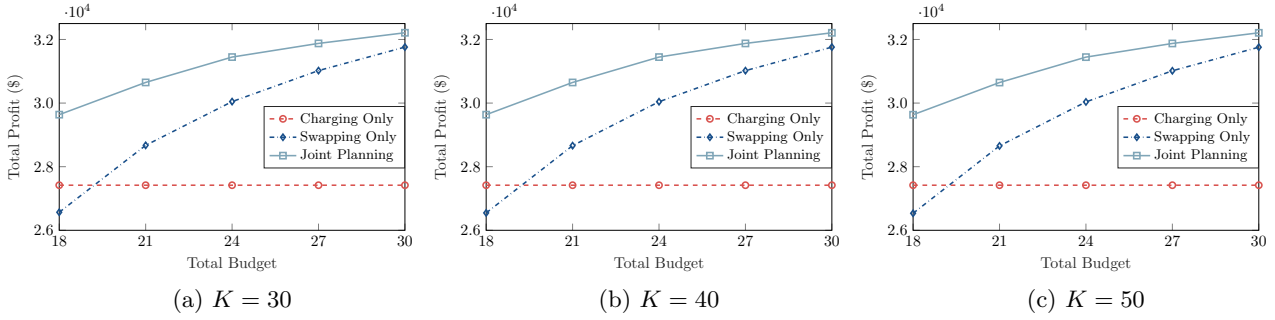


Figure E.12: Performance under different values of the queue capacity K .

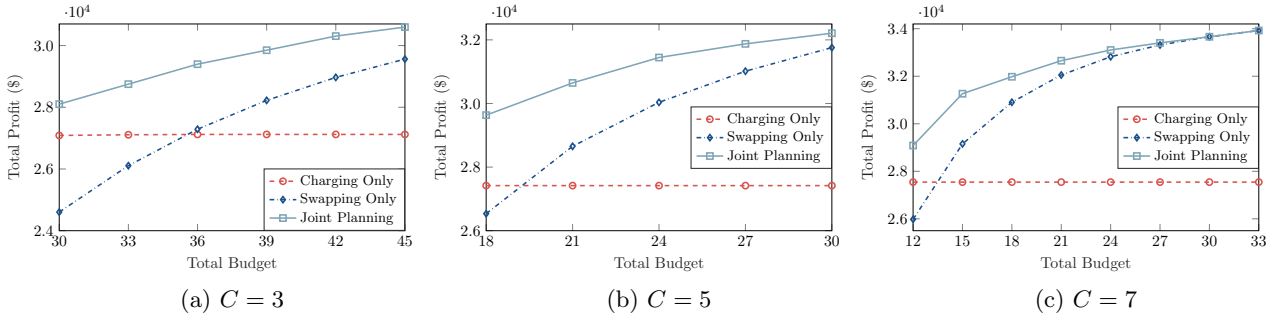


Figure E.13: Performance under different infrastructure configurations.

Appendix F. Results of Model Extensions

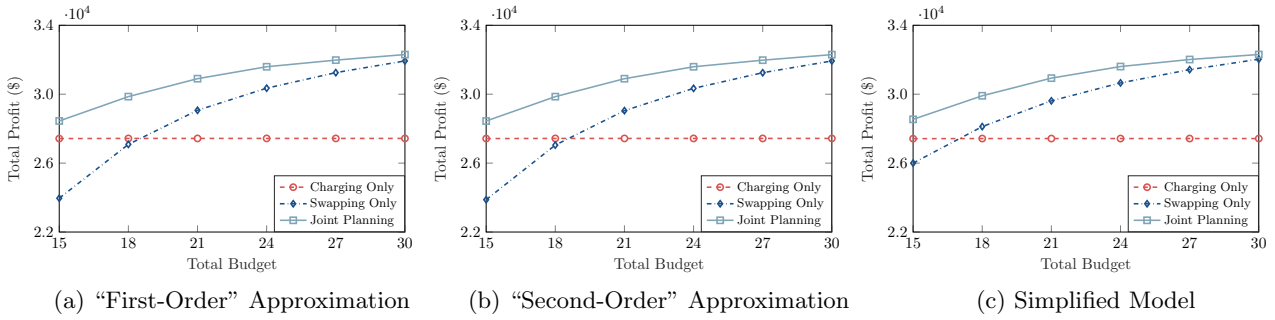


Figure F.14: Performance of the simplified and the extended models with a queue capacity of 10.

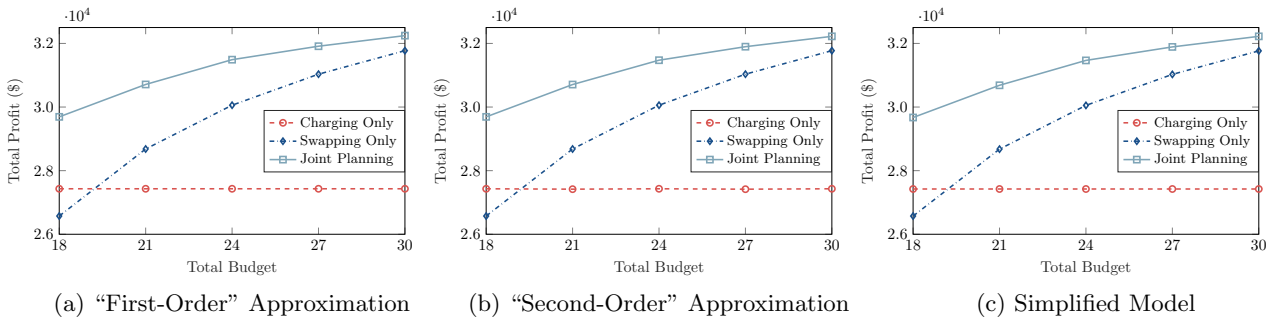


Figure F.15: Performance of the simplified and the extended models with a queue capacity of 30.

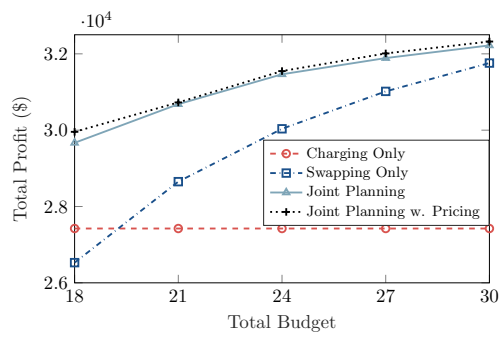


Figure F.16: Comparison between the performance with and without differentiated pricing.